Effects of nonlinearity and a new nonlinear resonance in two-path phonon transmittance in lattices with two-dimensional arrays of atomic defects

I. P. Koroleva (Kikot) [1,2] and Yu. A. Kosevich [1,3,4,*]
[1] *N. N. Semenov Federal Research Center for Chemical Physics of Russian Academy of Sciences, 4 Kosygin Street, Moscow 119991, Russian Federation*
[2] *National Research University Higher School of Economics, 34 Tallinskaya Str., Moscow 101000, Russian Federation*
[3] *Institute of Industrial Science, The University of Tokyo, Tokyo 153-8505, Japan*
[4] *Plekhanov Russian University of Economics, 36 Stremyanny per., Moscow 117997, Russian Federation*

(Received 8 October 2022; revised 21 March 2023; accepted 3 April 2023; published 22 May 2023)

The paper is devoted to analytical and numerical studies of the effects of nonlinearity on the two-path phonon interference in the transmission through two-dimensional arrays of atomic defects embedded in a lattice. The emergence of transmission antiresonance (transmission node) in the two-path system is demonstrated for the few-particle nanostructures, which allow us to model both linear and nonlinear phonon transmission antiresonances. The universality of destructive-interference origin of transmission antiresonances of waves of different nature, such as phonons, photons, and electrons, in two-path nanostructures and metamaterials is emphasized. Generation of the higher harmonics as a result of the interaction of lattice waves with nonlinear two-path atomic defects is considered, and the full system of nonlinear algebraic equations is obtained to describe the transmission through nonlinear two-path atomic defects with an account for the generation of second and third harmonics. Expressions for the coefficients of lattice energy transmission through and reflection from the embedded nonlinear atomic systems are derived. It is shown that the quartic interatomic nonlinearity shifts the antiresonance frequency in the direction determined by the sign of the nonlinear coefficient and enhances in general the transmission of high-frequency phonons due to third harmonic generation and propagation. The effects of the quartic nonlinearity on phonon transmission are described for the two-path atomic defects with a different topology. Transmission through the nonlinear two-path atomic defects is also modeled with the simulation of the phonon wave packet, for which the proper amplitude normalization is proposed and implemented. It is shown that the cubic interatomic nonlinearity red shifts in general the antiresonance frequency for longitudinal phonons independently of the sign of the nonlinear coefficient, and the equilibrium interatomic distances (bond lengths) in the atomic defects are changed by the incident phonon due to cubic interatomic nonlinearity. For longitudinal phonons incident on a system with the cubic nonlinearity, the new narrow transmission resonance on the background of a broad antiresonance is predicted to emerge, which we relate to the opening of the additional transmission channel for the phonon second harmonic through the nonlinear defect atoms. Conditions of the existence of the new nonlinear transmission resonance are determined and demonstrated for different two-path nonlinear atomic defects. A two-dimensional array of embedded three-path defects with an additional weak transmission channel, in which a linear analog of the nonlinear narrow transmission resonance on the background of a broad antiresonance is realized, is proposed and modeled. The presented results provide better understanding and detailed description of the interplay between the interference and nonlinearity in phonon propagation through and scattering in two-dimensional arrays of two-path anharmonic atomic defects with a different topology.

DOI: 10.1103/PhysRevE.107.054217

I. INTRODUCTION

Transmission of lattice waves through two-dimensional arrays of atomic-scale defects in crystal lattices and interfaces has attracted attention in view of various possible applications in nanoscience and nanotechnology. Since heat is carried mainly by acoustic lattice waves with high group velocity, investigation of such process can give important data for understanding and modeling of thermal conductivity in different metamaterials and thermal conductance through different material interfaces or metasurfaces [1,2]. Prediction of the impact of the extended, including two-dimensional (2D), arrays of lattice defects on the thermal conductivity and thermal interface conductance and on propagation of lattice waves in different frequency domains is the challenging task, which is important both for the theoretical and experimental studies of energy transport properties of crystal and phononic lattices and for different applications [3].

Among other dynamic phenomena, the existence of the transmission antiresonance, at which the plane lattice wave (phonon) is completely reflected by extended 2D atomic-scale defects with effective thickness much smaller than the relevant wavelength, such as a single crystal plane with

*Corresponding author: yukosevich@gmail.com

embedded atomic defects, is unexpected and interesting. This phenomenon is related to the destructive interference between the waves propagating through *two different wave paths*, through the defect atoms and through the host atoms. Transmission antiresonance and substantial change of the transmission spectrum due to the presence of a discrete defect plane (metasurface) in a bulk material can be observed both in acoustic systems (in transmission of phonons) and in optical systems (in transmission of photons). It is worth noting that in optical systems this effect is similar to the cancellation of the photon output due to the coalescence of the two single photons which interfere destructively after propagation through two different photon paths (the Hong-Ou-Mandel interference) [4–7]. Transmission antiresonances of photons in optical chains with defects and in metasurfaces with 2D nanostructures were studied, e.g., in Refs. [8,9]. Effects of destructive interference between two photons can be also observed in microwave systems [10].

Transmission antiresonances for acoustic phonons in crystals with embedded defect planes and in coupled atomic chains were first observed in Refs. [11,12]. The important feature of the described transmission antiresonances is the small (subwavelength) effective thickness of the planar crystal defect in comparison with the incident phonon wave length [11], which allows the continuous description of strong resonance reflection or absorption of acoustic waves at the nanoscale metasurfaces; see also Refs. [13–16]. The mechanism of the two-path phonon interference can be explained with the use of few-particles models (see Sec. II). The effects of acoustic phonon transmission antiresonances on thermal conductance through the crystal planes with 2D arrays of embedded atomic defects with complex structure were considered in Refs. [9,16–23]. It was shown that the sparse 2D arrays of defects or defect-atom nanoparticles, in which the defect atoms or defect-atom nanoparticles substitute only a part of the host atoms in a crystal plane and are located periodically, can result in substantial suppression of thermal interface conductance. Transmission antiresonances of long acoustic waves were also observed and studied in single- and multilayer elastic composites with local resonances of periodically embedded heavy particles, with a lattice constant two orders of magnitude smaller than the relevant wavelength [24,25]. In optical systems, transmission antiresonances at terahertz frequencies were observed in single- and double-layer 2D periodic arrays of metallic nanostructures on a transparent substrate (optical metamaterials and stereometamaterials); see, e.g., Refs. [26,27]. In such two-path periodic nanostructures, the lattice constants are also much smaller that the relevant wavelengths, and the two photon paths pass through the local metallic nanoplasmonic resonators and through the transparent substrate surrounding the nanoresonators. It is important to emphasize that the concept of destructive interference in the transmission through two different wave paths is universal and is applied to transmission antiresonances of waves of different nature, such as phonons, photons, and electrons; see Ref. [9] and Sec. II below.

Although destructive interference of the wave propagating through two different paths and the related phenomenon of total reflection (transmission antiresonance) is a linear effect, the nonlinearity (even weak) of the interatomic bonds in the atomic defect structure can substantially change the phonon transmittance. While the linear case can be resolved analytically in many cases (see, e.g., Refs. [16,21]), the presence of nonlinearity makes the task much more difficult and multilateral [28]. For instance, the phonon transmission coefficient cannot be explicitly calculated within the atomistic Green's function approach for the anharmonic (nonlinear) interface [29–33]. This fact makes the analysis, within the nonlinear lattice-dynamics approach, of the effects of nonlinearity on phonon transmittance through the embedded two-path atomic defects with different internal structure one of the main motivations of the present study. The influence of quartic nonlinearity on the transmission spectrum in an optical chain with a side nonlinear defect was studied in Ref. [8], and it was shown that the antiresonance frequency is shifted and transmission line shape is changed by the nonlinearity. However, as in the most of the papers dedicated to the study of the effects of nonlinearity, the rotating-wave approximation, in which the third harmonics is neglected, was used in Ref. [8]. This approximation is well applied in optical systems but cannot be fully justified in nonlinear phononics because of the presence of higher harmonics in lattice dynamics. The contribution of the multi- and subharmonic phonon transmission to the Kapitza conductance between crystals with very different vibrational spectra and with nonlinear interface resonant layer was calculated in the continuum limit in Ref. [28]; see also Ref. [31]. As for the crystal lattices with discrete 2D arrays of atomic defects, to the best of our knowledge only the molecular dynamics (MD) simulations of such nonlinear systems have been reported in Refs. [16,18,19].

The present paper is dedicated to the investigation of the effects of the cubic and quartic nonlinearity of interatomic bonds in 2D arrays of atomic defects embedded in a lattice on the two-path phonon interference and transmission beyond the rotating-wave approximation. In the proposed nonlinear lattice-dynamics approach, the full system of nonlinear algebraic equations for the amplitudes of the transmission through and reflection at nonlinear two-path atomic defects with an account for the generation of second and third harmonics is derived. The nonlinear algebraic equations are further solved numerically. We show that in the nonlinear case the antiresonance is still present, but the shape of spectral lines and antiresonance frequency can be drastically changed and the antiresonance is accompanied by the enhancement of phonon transmission in high-frequency domain due to higher harmonics generation and propagation. The effect of higher harmonics generation is important in general; for instance, the harmonics generation at the nanoscale allows to interrogate matter in extremely confined volumes [34] while modern nonlinear optical technique of second harmonic generation is employed to probe the biologically relevant lipid bilayers and other living systems [35].

The phenomenon of the two-path antiresonance can be useful while constructing the atomic-scale metamaterials with the predictable phonon transmittance. Since our techniques can be applied to any realistic system with the two-path atomic defects, we consider several different systems. The destructive phonon interference is the most notable when the defect atoms are heavier that host lattice atoms, but the opposite case is also considered. One of the considered systems is the 2D array of heavy atomic defects (a layer of Ge-like atoms) in a simple cubic lattice of light (Si-like) atoms, which can be regarded as a quasi-one-dimensional (1D) lattice for the normal phonon incidence. Another model system is a quasi-1D lattice of atomic defects with weak coupling and/or light masses. An example of such system can be the 2D array of light atomic defects (a single layer of Si-like atoms) in a simple cubic lattice of heavy (Ge-like) atoms. Both crystal lattices with an embedded 2D array can be regarded asquasi-1D atomic chains for the normal phonon incidence, and their quasi-1D model is shown in Fig. 2 below. In the system with the heavy atomic defects, both the antiresonance frequency and the high-frequency domain are influenced by the quartic nonlinearity. In the system with the weak coupling, the antiresonance frequency almost does not depend on the quartic nonlinearity, but the shape of transmission spectral line changes drastically. It is worth noting in this regard that the two-path transmission antiresonances in sparse 2D arrays of atomic defects are also present in the case of oblique phonon incidence if the deviation from the normal incidence is not very large [36].

In the systems with the cubic nonlinearity for the incident longitudinal wave, a new narrow transmission resonance on the background of a broad antiresonance can appear, which we relate to the opening of the additional transmission channel for a phonon second harmonic through the embedded nonlinear atomic defects. We determine the conditions of the existence of the new nonlinear transmission resonance and demonstrate them for different embedded two-path nonlinear atomic systems. We also propose and model the 2D array of embedded three-path defects with an additional weak transmission channel, in which a linear analog of the nonlinear narrow transmission resonance on the background of a broad antiresonance is realized. The linear analog helps to understand the origin of the new nonlinear resonance. It is worth mentioning that the narrow transmission resonance close to the antiresonance frequency, such as shown in Figs. 13, 14, and 16, recalls the narrow pass band in the transmission stop band, which can appear in phononic crystals made of periodic arrays of thin-walled hollow elastic cylinders embedded in water or air; see Refs. [37–39].

We also describe transmission antiresonances in a topologically different embedded nonlinear atomic system, which we relate to the structure of the two-path 2D planar defect in a diamond-like cubic lattice with two host atoms per unit cell. We consider the corresponding two-monolayer atomic defect as a realistic model for the 2D array of defects, formed by heavy Ge atoms embedded in a diamond-like cubic lattice of lighter Si atoms; see Ref. [21]. Two antiresonances are present in the transmission spectrum in such a two-path two-monolayer 2D array of defects, and here we analyze the effects of quartic nonlinearity on them. It is important to emphasize that in the linear case the two phonon transmission antiresonances in the two-path two-monolayer 2D system have the same destructive-interference origin as the two photon transmission antiresonances in the two-path double-layer stereometamaterials [27].

Within the proposed nonlinear lattice-dynamics approach, the spectra of lattice waves transmission can be calculated not only for single-frequency extended plane waves (phonons) but also for the Gaussian phonon wave packets (WPs) with finite frequency domains and finite spatial localization (coherence) lengths, which are routinely simulated within the molecular dynamics approach [40]. Simulations of WP transmission in a different nonlinear atomic system have been reported in several papers; see, e.g., Refs. [8,16,18,19]. However if one intends to compare these results with the lattice-dynamics prediction for the transmission of plane waves in the nonlinear atomic system, the very important question of WP amplitude normalization arises because the change of WP amplitude (or, the same, of WP energy) induces the change of the effective nonlinear coefficient. We propose and apply the method of WP amplitude normalization, which properly determines the WP amplitude, energy, and nonlinear parameter, and provides a good conformity between the results of lattice-dynamics calculations of the plane wave and WP transmission spectra.

The paper is organized as follows. In Sec. II we demonstrate the underlying mechanism of the transmission antiresonance on the example of several two-path few-particle systems and compare the considered systems with the one-path two-particle system, which was proposed earlier as a classical analogy of the Fano resonance. In Sec. III and Appendixes A, B, and C, we describe our lattice-dynamics approach, based on a system of nonlinear algebraic equations for the complex transmission and reflection amplitudes of the normal-incident (longitudinal) lattice waves at the 2D two-path nonlinear atomic systems embedded into the (simple cubic) lattice. In Sec. IV we present the results on the effect of quartic nonlinearity of the embedded atomic system on the transmission of the plane wave or phonon WP through such system. In Sec. V we present the results of the effect of cubic nonlinearity of the embedded atomic system on the (longitudinal) plane wave transmission through and reflection from such a system. Here we also describe the transmission spectra with the new nonlinear sharp transmission resonance or antiresonance, produced by the phonon second harmonic generated in the embedded atomic defect system with cubic nonlinearity. In Sec. VI we describe the effects of quartic nonlinearity on the transmission through the topologically different 2D two-path atomic system, embedded in a lattice with two host atoms per unit cell, which is characterized by the emergence of two antiresonances. In the Conclusion we summarize the main results presented in the paper.

II. MECHANISM OF THE TWO-PATH DESTRUCTIVE INTERFERENCE

It is easy to demonstrate the mechanism on the example of a few-particle system. We consider a system consisting of four particles; see Fig. 1(a). Hereinafter blue lines denote linear bonds while green zig-zags denote nonlinear bonds. All particles (atoms) beside the d-atom are connected by linear (blue) bonds, and the d-atom is connected by nonlinear (green) bonds with the nearest neighbors. The mass of the 0-atom is m_0, the mass of the d-atom is m_d, and the mass of the side particles (1-st and -1-st) is m. Rigidity of the bonds connecting the 0-atom (blue ones) with its neighbors is k_0, while linear rigidity of the bonds connecting the defect atom with its neighbors is k_d (green ones), and these bonds in general also have the nonlinear contribution. The Lagrangian

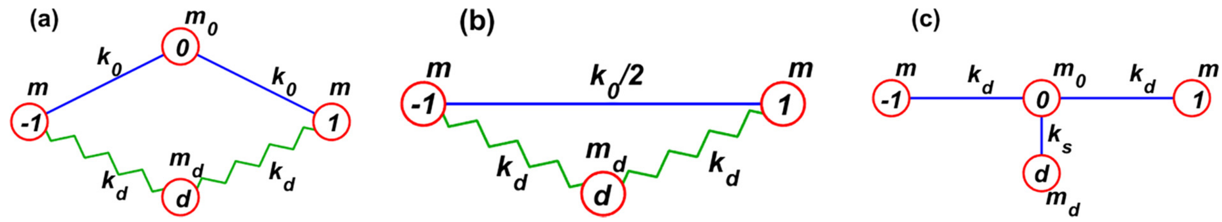

FIG. 1. Structure of two-path few-particle systems.

of the considered four-particle system is the following:

$$\mathcal{L} = \sum_{i=-1}^{+1} \frac{m\dot{u}_i^2}{2} + \frac{m_0\dot{u}_0^2}{2} + \frac{m_d\dot{u}_d^2}{2} - \left(\frac{1}{2}k_0(u_0-u_1)^2 + \frac{1}{2}k_0(u_0-u_{-1})^2 + \frac{1}{2}k_d(u_d-u_{-1})^2 + \frac{1}{2}k_d(u_d-u_1)^2 + \frac{1}{4}K_4(u_d-u_{-1})^4 + \frac{1}{4}K_4(u_d-u_1)^4\right), \tag{1}$$

where the nonlinear coefficient K_4 describes the quartic nonlinearity of the d-atom bonds with the nearest neighbors.

Other few-particle two-path atomic systems can be built from the one above: (a) by putting $m_0 = 0$, which is equivalent to the introduction of the direct bond between the -1-st and 1-st atoms with the $k_0/2$ force constant [Fig. 1(b)]; and (b) by introducing the direct bond k_s between the 0- and d-atoms and "cutting" the k_d bonds, which produces the Helmholtz-type atomic side-attached oscillator with mass m_d and k_s coupling with the three-atom chain [Fig. 1(c)]; see also Ref. [9]. All these two-path few-particle systems are different from the two weakly coupled on-site oscillators connected in series, which present an apparent one-path system that was proposed for the classical-mechanics modeling of the Fano-like sharp asymmetric line shape in the *absorption and scattering spectra*; see, e.g., Refs. [41–46].

All the aforementioned two-path few-particle systems, being embedded in an atomic chain such as shown in Fig. 2, are characterized by the presence of the *transmission antiresonance* (zero transmission dip) within the chain phonon band. With the few-particle systems, shown in Fig. 1, the transmission antiresonance can be modeled with the frequency at which the amplitude of the 1-st particle turns to zero when the harmonic driving force $\propto \cos(\omega t)$ is applied to the -1-st particle. The aforementioned one-path two-particle systems, such as that discussed in Refs. [41–46], do not produce such transmission antiresonance.

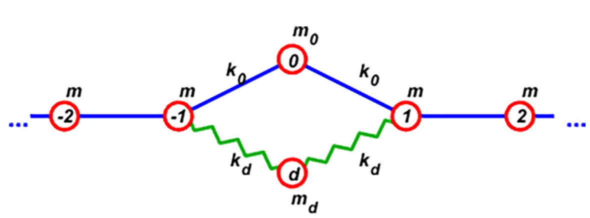

FIG. 2. Quasi-1D model of lattice system with the two-path nonlinear atomic defect with two connected-in-parallel atoms and bonds.

Antiresonance in two-path few-particle systems

First, we consider the linear case when it is easy to demonstrate and explain the phenomenon of the transmission antiresonance. One can just let nonlinear coefficient be zero $K_4 = 0$ in Eq. (1). For convenience, we introduce the following notations: $\omega_1^2 = k_0/m$, $\omega_0^2 = k_0/m_0$, $\omega_d^2 = k_d/m_d$, $\omega_2^2 = k_d/m$.

When the left, -1-st, particle is exposed to an external harmonic driving force $Am\cos(\omega t)$, the dynamics of the system with Lagrangian (1) is governed by the following equations:

$$\ddot{u}_0 + \omega_0^2(2u_0 - u_{-1} - u_{+1}) = 0, \tag{2}$$

$$\ddot{u}_d + \omega_d^2(2u_d - u_1 - u_{-1}) = 0, \tag{3}$$

$$\ddot{u}_1 + \omega_1^2(u_1 - u_0) + \omega_2^2(u_1 - u_d) = 0, \tag{4}$$

$$\ddot{u}_{-1} + \omega_1^2(u_{-1} - u_0) + \omega_2^2(u_{-1} - u_d) = A\cos\omega t. \tag{5}$$

We are looking for the harmonic solution in the form

$$u_{-1} = C_{-1}e^{i\omega t}, \quad u_1 = C_1 e^{i\omega t}, \quad u_d = C_d e^{i\omega t}, \quad u_0 = C_0 e^{i\omega t}. \tag{6}$$

Using Eqs. (2)–(5) with these substitutions, we obtain a linear system for the coefficients C_i. Resolving it, we get an equation on the amplitude of the right (1-st) particle:

$$C_1\left[-\omega^2 + \omega_1^2 + \omega_2^2 - 2\left(\frac{\omega_0^2\omega_1^2}{2\omega_0^2 - \omega^2} + \frac{\omega_2^2\omega_d^2}{2\omega_d^2 - \omega^2}\right)\right] = \frac{A}{-\omega^2 + \omega_1^2 + \omega_2^2}\left(\frac{\omega_0^2\omega_1^2}{2\omega_0^2 - \omega^2} + \frac{\omega_2^2\omega_d^2}{2\omega_d^2 - \omega^2}\right). \tag{7}$$

So we get an analytical expression for the amplitude of the right particle depending on the frequency ω and reduced amplitude A of the external harmonic driving force, which is applied to the left atom. In other words, this equation describes the portion of the external driving force that has passed through the two-path atomic system.

Several resonances exist in the system. The phenomenon of the transmission antiresonance corresponds to the case of $C_1 = 0$ when the right atom does not move in spite of the forcing of the left atom. We can find the antiresonance frequency from Eq. (7). The amplitude $C_1 = 0$ if the following equation holds:

$$\frac{\omega_0^2\omega_1^2}{2\omega_0^2 - \omega_R^2} + \frac{\omega_2^2\omega_d^2}{2\omega_d^2 - \omega_R^2} = 0, \tag{8}$$

from which we obtain the expression for the antiresonance frequency:

$$\omega_R{}^2 = 2\frac{\omega_0^2\omega_d^2(\omega_1^2+\omega_2^2)}{\omega_0^2\omega_1^2+\omega_2^2\omega_d^2}. \tag{9}$$

The defect depicted on Fig. 1(b) can be considered as a limiting case of the defect shown in Fig. 1(a) by setting $m_0 = 0$, that is $1/\omega_0^2 = 0$. This means that Eq. (9) will be written as

$$\omega_R{}^2 = 2\frac{\omega_d^2(\omega_1^2+\omega_2^2)}{\omega_1^2}.$$

The case of the defect depicted in Fig. 1(c) is different. Equation (7) is written in this case as

$$C_1 = A\frac{\omega_0^2\omega_1^2}{\omega_1^2-\omega^2}\cdot\frac{\omega_d^2-\omega^2}{[(\omega_1^2-\omega^2)(\omega_s^2-\omega^2)-2\omega_0^2\omega^2](\omega_d^2-\omega^2)-\omega_d^2\omega_s^2(\omega_1^2-\omega^2)}, \tag{10}$$

with $\omega_d^2 = k_s/m_d$, $\omega_s^2 = k_s/m_0$, $\omega_0^2 = k_0/m_0$, $\omega_1^2 = k_0/m$. Equation (10) shows that for the defect depicted on Fig. 1(c), the antiresonance frequency is $\omega_R = \omega_d = \sqrt{k_s/m_d}$, provided that the product $\omega_d\omega_s$ is nonzero and ω_d is finite. In the case of zero product $\omega_d\omega_s$, which corresponds to zero bond stuffiness k_s or infinite mass m_d or m_0, the transmission antiresonance is absent. Zero bond stiffness k_s describes a one-path system of three coupled atoms, the -1, 0, and $+1$. A one-path system is realized for finite stiffness k_s, zero mass m_d, and infinite ω_d when a massless spring with stiffness k_s is attached to the 0-th atom in the three-atom one-path chain. Infinite mass m_d describes the 0-th atom as an oscillator with an on-site frequency ω_s in a one-path three-atom system. Infinite mass m_0 describes the 0-th atom as a phonon-impenetrable obstacle when $u_1 = 0$ for all frequencies (including the resonance at $\omega = \omega_1$ with an account for oscillations damping) because of $\omega_0 = \omega_s = 0$, as Eq. (10) shows.

The notion of the Fano resonance [47] covers a great variety of different resonance effects; see, e.g., Refs. [43,45,48] for recent reviews. However, we do not consider the described phenomenon of the transmission antiresonance as the Fano resonance, as was done, for instance, in Ref. [8], because the transmission antiresonance and the Fano effect in the absorption and scattering spectra generally have different origins. The considered phonon transmission antiresonance is a result of the destructive interference of the waves propagating through the two different wave paths in the atomic-scale metastructure embedded in a crystal, in the *absence of wave damping* as well; see also Refs. [9,11,16–20,22]. It is also important that in the considered transmission antiresonances, the states in both wave paths are in the phonon continuum of the system (the resonance states): there is no interference between the localized and continuum states, which is considered to be the main source of the Fano resonance [41–43,49]. Transmission antiresonances were also observed and studied in acoustic metamaterials without direct connection with the Fano resonance; see, e.g., Ref. [25] for a recent review. On the other hand, the classical Fano effect of a sharp asymmetric line shape with a narrow dip in the absorption spectrum (the frequency of almost zero total loss) is well described by the spectrally narrow cancellation of the total loss in a system of two connected-in-series weakly coupled oscillators or two weakly coupled modes with very different damping rates (finite and almost zero of the "bright superradiant" and "dark subradiant" modes), which is accompanied by the narrow *transmission resonance*, instead of transmission node, and therefore this effect is associated with the classical analog of electromagnetically induced transparency, see, e.g., Ref. [50]. [In fact, the model with two weakly coupled oscillators (optical phonons) with very different damping rates (finite and almost zero) was proposed for the first time in Ref. [51] for the modeling of a narrow dip in the infrared absorption and reflection spectra in high-dielectric-constant materials without making the connection to Fano's paper; see also Ref. [52].] It is important to underline in this connection that the transmission antiresonance, which is presented in Ref. [42], clearly shows that in the considered electron waveguide with an asymmetrically embedded quantum dot there are two different electron wave paths around the quantum dot, which become identical for the symmetric position of the quantum dot on the central line of the waveguide when the antiresonance disappears. This observation confirms the universality of the destructive-interference origin of transmission antiresonances of waves of different nature, including electron waves, in two-different-path structures.

For the system shown in Fig. 1(a), the oscillation wave, which passes through the 0-atom, "annihilates" at the transmission antiresonance with the wave that passes through the d-atom. From the physical point of view, this can be explained by the fact that when there is only one wave path (or two identical wave paths), the transmitted wave cannot be blocked in a finite (compact) few-particle system by the superposition (interference) with another wave. The celebrated total Bragg reflection, caused by one-path destructive interference, can be realized only in infinite periodic systems.

The absence of the transmission antiresonance in the one-path few-particle system can also be demonstrated with the use of Eqs. (8) and (10). The one-path case corresponds to the limit when the two paths in Fig. 1(a) are identical, that is, when $m_d = m_0$, $k_d = k_0$ and $\omega_d = \omega_0$, $\omega_1 = \omega_2$ in result. Then Eq. (8) transforms into the equation

$$\frac{2\omega_0^2\omega_1^2}{2\omega_0^2-\omega_R^2} = 0, \tag{11}$$

which obviously has no solution for the finite ω_R. The absence of the solution $u_1 = C_1 = 0$ for finite frequency in the case of $\omega_d = \omega_0$ and $\omega_1 = \omega_2$ also follows directly from Eq. (7). As was explained above, Eq. (10) also shows the absence of transmission antiresonance in the cases of zero bond stiffness k_s and zero or infinite mass m_d in the system shown in Fig. 1(c), and all these cases describe different one-path three-particle systems. The inclusion of the on-site potentials for the particles in such one-path few-particle systems, similar to that discussed in Refs. [41–46], also does not produce transmission antiresonance in the corresponding systems.

It is important that the two-path transmission antiresonance can be spectrally broad and may have an almost symmetric line shape, such as the antiresonances shown in Figs. 18(a) and 18(b). Narrow, Fano-like, antiresonances with sharp asymmetric line shapes are present in the transmission spectra through the systems with two different (asymmetric) paths, weakly split in eigenfrequencies or damping constants, or when one of the paths is weak (rare in average), such as the systems with the transmission spectra shown in Figs. 5 and 7 in Ref. [16]. Examples of the transmission spectra with sharp asymmetric in general line shapes, which we relate with the opening of the additional transmission channel for a relatively weak phonon second harmonic through the embedded nonlinear defect atoms, are presented in Sec. V. The narrow Fano-like transmission antiresonances with asymmetric line shapes can be considered as a particular case of the antiresonance in the transmission through the embedded system with two very different wave paths, such as the system shown in Fig. 2.

One may ask: how does nonlinearity influence the transmission antiresonance? For a nonlinear system with the Lagrangian (1), the transmission spectrum of the four-particle system (see Fig. 3) can be obtained within the approach for the two-path defects in a chain, which will be described in the following section. As one can see in Fig. 3, the nonlinearity shifts the antiresonance frequency. However, the antiresonance survives in the presence of relatively weak nonlinearity.

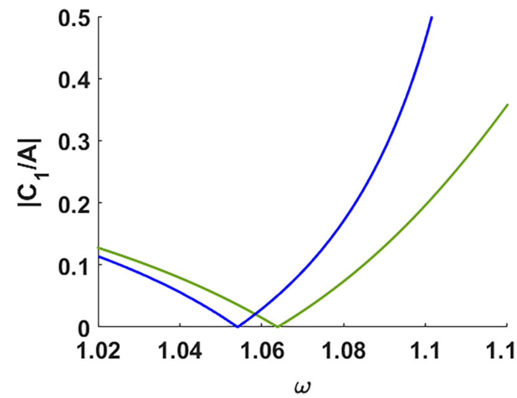

FIG. 3. Spectrum of normalized amplitude of 1-st particle in linear (blue line) and nonlinear (with parameter $K_4A^2 = 0.005$, green line) four-particle systems shown in Fig. 1(a), for $k_0 = k_d = 0.5$, $m_0 = 0.5$, $m_d = 1.3$, $m = 1$. The lines are indicated from left to right.

III. NONLINEAR LATTICE-DYNAMICS APPROACH FOR THE STUDY OF PLANE WAVE TRANSMISSION AND REFLECTION IN QUASI-1D CHAIN WITH NONLINEAR ATOMIC DEFECT

Let us consider quasi-1D chain with the embedded two-path defect; see Fig. 2. Such system models a three-dimensional crystal with one defect crystal plane (the chain axis corresponds to the direction normal to defect plane) with alternating in checkerboard order the host and defect atoms. For example, these can be heavy Ge-like atoms in a simple cubic crystal lattice of Si-like atoms, with one atom per unit cell. A more realistic defect crystal plane with sparse distribution of Ge atoms in a diamond Si lattice with two atoms per unit cell will be considered in Sec. IV. Due to the sparse 2D distribution of atomic defects in the crystal plane, there are two paths for the lattice wave: through the defect atom and through the host atom. The model is rather general and may be applied to many other crystal systems as well as for the study of general mechanism of lattice energy transfer through defect crystal planes; see also Refs. [9,16–18,21]. The system is described by the following Fermi-Pasta-Ulam (FPU) Lagrangian:

$$\begin{aligned}\mathcal{L} = &\sum_{i=-\infty}^{-1}\frac{m\dot{u}_i^2}{2}+\frac{m_0\dot{u}_0^2}{2}+\frac{m_d\dot{u}_d^2}{2}+\sum_{i=1}^{\infty}\frac{m\dot{u}_i^2}{2}-\left(\sum_{i\neq 0,-1}\frac{k_{\rm norm}(u_i-u_{i-1})^2}{2}+\frac{k_0(u_0-u_{-1})^2}{2}+\frac{k_0(u_0-u_1)^2}{2}\right.\\ &+\frac{k_d(u_d-u_{-1}-\Delta_1)^2}{2}+\frac{K_3(u_d-u_{-1}-\Delta_1)^3}{3}+\frac{K_4(u_d-u_{-1}-\Delta_1)^4}{4}\\ &\left.+\frac{k_d(u_1-u_d-\Delta_2)^2}{2}+\frac{K_3(u_1-u_d-\Delta_2)^3}{3}+\frac{K_4(u_1-u_d-\Delta_2)^4}{4}\right). \qquad (12)\end{aligned}$$

This is the most general case of a system with the cubic (K_3) and quartic (K_4) nonlinearities of the embedded atomic defects. Here the variables Δ_1 and Δ_2 describe the change of the equilibrium interatomic bond lengths caused by cubic anharmonicity, which is known from the dynamics of nonlinear oscillations [53] and which will be discussed in Sec. V.

We are looking for the solution with higher harmonics generation by taking into account that the nonlinear defect generates additional waves with double and triple frequencies (the second and third harmonics):

$$u_n = Ae^{ikan-i\omega t}+Are^{-ikan-i\omega t}+Ar_2e^{-ik_2an-2i\omega t}+Ar_3e^{-ik_3an-3i\omega t}+\text{c.c.}, n\leqslant -2, \qquad (13)$$

$$u_n = Ate^{ikan-i\omega t}+At_2e^{ik_2an-2i\omega t}+At_3e^{ik_3an-3i\omega t}+\text{c.c.}, n\geqslant 2 \qquad (14)$$

with A being an amplitude of the incident plane wave with frequency ω, and a being a period of the lattice. Here t, t_2, t_3 and r, r_2, r_3 are, respectively, the normalized transmission and reflection amplitudes of the main, second and third phonon harmonics. The frequency and wave number obey the following dispersion relations (assuming that the nonlinearity of the defect atoms bonds is relatively small):

$$\omega^2 = \frac{4k_{\text{norm}}}{m}\sin^2\frac{ka}{2}, \tag{15}$$

$$(2\omega)^2 = \frac{4k_{\text{norm}}}{m}\sin^2\frac{k_2 a}{2}, \tag{16}$$

$$(3\omega)^2 = \frac{4k_{\text{norm}}}{m}\sin^2\frac{k_3 a}{2}. \tag{17}$$

The atoms neighboring the structural defect, which are the 1-st and the -1-st atoms, oscillate with the same frequency and with different in general amplitudes:

$$u_0 = A(A_0 e^{-i\omega t} + t_{2,0}e^{-2i\omega t} + t_{3,0}e^{-3i\omega t} + \text{c.c.}), \tag{18}$$

$$u_{-1} = A(A_{-1} e^{-i\omega t} + r_{2,-1}e^{-2i\omega t} + r_{3,-1}e^{-3i\omega t} + \text{c.c.}), \tag{19}$$

$$u_{+1} = A(t_1 e^{-i\omega t} + t_{2,1}e^{-2i\omega t} + t_{3,1}e^{-3i\omega t} + \text{c.c.}), \tag{20}$$

$$u_d = A(D_1 e^{-i\omega t} + D_2 e^{-2i\omega t} + D_3 e^{-3i\omega t} + \text{c.c.}). \tag{21}$$

We have six equations of motion for the $u_{-2}, \ldots, u_2, u_d$ displacements, which follow from the Lagrangian (12). Substituting the expressions (13)–(14) and (18)–(21) into these equations and equating the coefficients in front of $e^{-i\omega t}$, $e^{-2i\omega t}$, and $e^{-3i\omega t}$, we get 20 algebraic equations for 20 complex amplitudes (see Appendix A). The problem is to solve this algebraic system for each value of frequency and get the dependence of the transmitted and reflected wave amplitudes on the frequency.

We suppose that the effect of nonlinearity is relatively small, and the amplitudes of the third harmonics are much smaller than the amplitudes of the fundamental-frequency waves: $(t_{30}, t_3, r_3, r_{3,-1}, t_{31}, D_3) \ll (r, t, A_0, A_{-1}, t_1, D_1)$. We consider in detail the equation for defect atom displacement, in which we omit terms of the second and higher orders:

$$\begin{aligned} &m_d(-D_1\omega^2) + k_d(2D_1 - A_{-1} - t_1) \\ &\quad + K_4A^2[3(D_1 - A_{-1})^2(D_1{}^* - A_{-1}{}^*)] \\ &\quad + K_4A^2[3(D_1 - t_1)^2(D_1{}^* - t_1{}^*)] = 0. \end{aligned} \tag{22}$$

The nonlinear physical parameter is the product K_4A^2, which remains in the equations of nonlinear lattice dynamics. In the quasiharmonic approximation, we suppose that this parameter is small, $K_4A^2 \ll k_{\text{norm}}$. The obtained full system of algebraic equations, which describes the transmission of the plane wave through the embedded nonlinear atomic defect, can be found in Appendix A. This system has been solved numerically.

The nonlinear phonon transmission T and reflection R coefficients were calculated in the quasiharmonic approximation using the following expressions:

$$\begin{aligned} T &= |t|^2 + 4|t_2|^2\text{Re}\left(\sqrt{\frac{w_{\max}^2 - 4w^2}{w_{\max}^2 - w^2}}\right) \\ &\quad + 9|t_3|^2\text{Re}\left(\sqrt{\frac{w_{\max}^2 - 9w^2}{w_{\max}^2 - w^2}}\right), \end{aligned} \tag{23a}$$

$$\begin{aligned} R &= |r|^2 + 4|r_2|^2\text{Re}\left(\sqrt{\frac{\omega_{\max}^2 - 4\omega^2}{\omega_{\max}^2 - \omega^2}}\right) \\ &\quad + 9|r_3|^2\text{Re}\left(\sqrt{\frac{\omega_{\max}^2 - 9\omega^2}{\omega_{\max}^2 - \omega^2}}\right), \end{aligned} \tag{23b}$$

which take into account the finite width of the phonon transmission band with maximal frequency ω_{max} and phonon group velocity in a monatomic chain. Equations (23a) and (23b) explicitly take into account that lattice waves of the second and third harmonics do not transfer the oscillation energy above the maximal phonon frequency $\omega_{max} = 2\sqrt{\frac{k_{\text{norm}}}{m}}$ (in the phonon stop band of the chain). The derivation of Eqs. (23a) and (23b) is given in Appendix C.

The sum of the transmission and reflection coefficients determines the total normalized flux of phonon energy in incident and reflected lattice waves P_{ph}:

$$\begin{aligned} P_{ph} = T + R &= |t|^2 + 4|t_2|^2\text{Re}\left(\sqrt{\frac{w_{\max}^2 - 4w^2}{w_{\max}^2 - w^2}}\right) \\ &\quad + 9|t_3|^2\text{Re}\left(\sqrt{\frac{w_{\max}^2 - 9w^2}{w_{\max}^2 - w^2}}\right) \\ &\quad + |r|^2 + 9|r_2|^2\text{Re}\left(\sqrt{\frac{w_{\max}^2 - 4w^2}{w_{\max}^2 - w^2}}\right) \\ &\quad + 9|r_3|^2\text{Re}\left(\sqrt{\frac{w_{\max}^2 - 9w^2}{w_{\max}^2 - w^2}}\right). \end{aligned} \tag{24}$$

Conservation of lattice energy requires that $P_{ph} = 1$. This requirement will be used for the control of the accuracy of numerical simulations.

IV. INFLUENCE OF QUARTIC NONLINEARITY ON PHONON TRANSMISSION

In this section we consider several systems with different parameters. Hereinafter we use dimensionless units in which $m = 1$, $k_{\text{norm}} = 1$, $a = 1$. Some of the considered systems (described by sets of parameters) model a real crystal with defect plane, and some of them are just model systems. The latter ones are useful for illustrating some effects and enable us to make general conclusions.

Case 1. The first considered system is a model system of a lattice with the two-path defect, shown in Fig. 2, where the defect atom is four times heavier that the host atoms. Dimensionless parameters of the defect are the following: $k_0 = 0.5$, $k_d = 0.5$, $m_0 = 0.5$, $m_d = 2$. Figure 4(a) shows that the quartic nonlinearity leads to the shift of antiresonance frequency and to the change of the transmission spectrum line shape in the domain of higher frequencies.

To control the correctness of our approximations and accuracy of numerical calculations, we also consider the spectrum of the sum of nonlinear transmission and reflection coefficients, the total normalized flux of lattice energy in incident and reflected waves P_{ph}, Eq. (24), which should be equal to

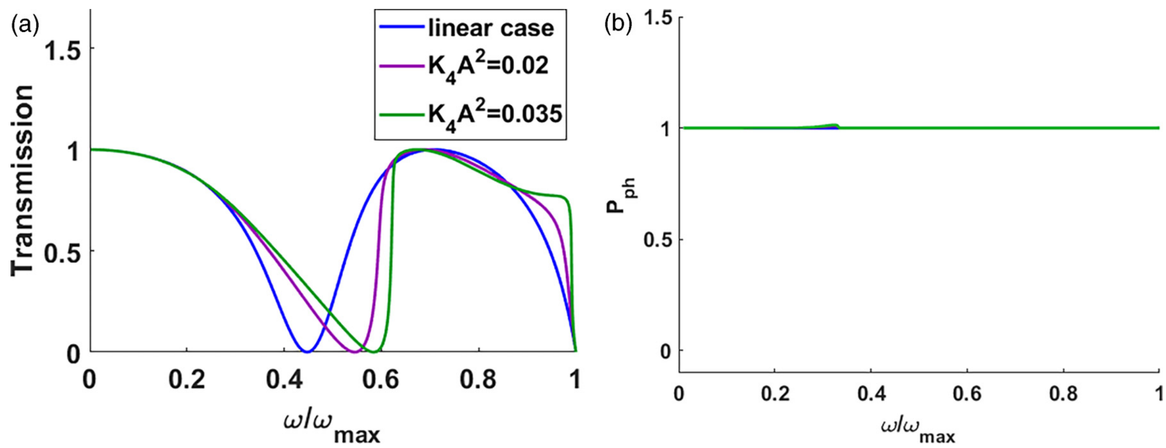

FIG. 4. (a) Spectrum of transmission coefficients and (b) total normalized flux of lattice energy in incident and reflected waves P_{ph}, given by Eq. (24), in a model system, shown in Fig. 2, with the defect atom four times heavier than host atoms. In the legend in (a), the lines are indicated from left to right.

one due to energy conservation in the Hamiltonian system. Figure 4(b) shows that this equality holds very accurately. We have also calculated the spectrum of the total flux P_{ph} for other systems, and in all the considered systems the phonon energy is conserved in our simulations.

Case 2. The mass of the defect atom is 2.6 times heavier than the mass of host atoms. This system models the simple cubic crystal of Si-like atoms with a 2D defect layer consisting of Si-like and Ge-like atoms; see also [18,19]. The used parameters are $k_0 = k_d = 0.5$, $m_0 = 0.5$, and $m_d = 1.3$. Figure 5 shows that even a relatively small quartic nonlinearity shifts the antiresonance frequency (in the direction determined by the sign of nonlinear coefficient K_4), but the influence of the quartic nonlinearity on the line shape is negligible in such a system. The quartic-nonlinearity-induced shift of the antiresonance frequency is qualitatively similar to that obtained in [8] devoted to wave propagation in a nonlinear optical chain with the defects with on-site quartic nonlinearity, but our transmission spectra take explicitly into account the generation and propagation of the third (and second; see below) phonon harmonics, which cannot be described in the rotating-wave approximation that was used in Ref. [8].

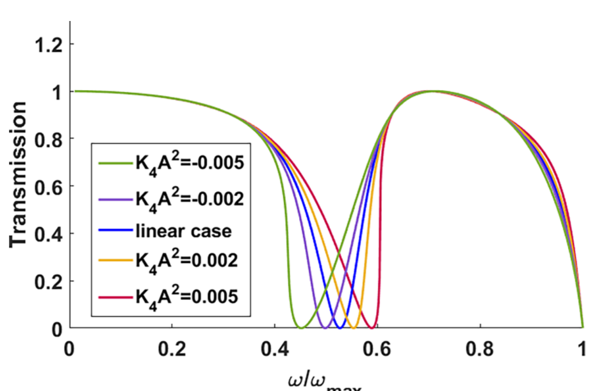

FIG. 5. Spectrum of the transmission coefficient in a simple cubic lattice of Si-like atoms with a defect layer of Ge-like and Si-like atoms with mass ratio 2.6. In the legend the lines are indicated from left to right.

Case 3. The system with a weak coupling. This structure models the 0-th atom, which is weakly coupled with the lattice, and there is another wave path through the nonlinear bond between the −1-st and 1-st atoms (formally, with the defect with zero mass, $m_d = 0$, the −1-st and 1-st atoms are directly connected through the nonlinear bond with force constant $k_d/2$ in the linear limit). That is, we consider the defect shown in Fig. 2 with $k_0 = 0.07$, $k_d = 0.28$, $m_0 = 1$, $m_d = 0$.

Figure 6 shows that the quartic nonlinearity in this system does not shift the antiresonance frequency but changes the line shape in both the low-frequency and high-frequency domains. Although it is a model system, it enables us to detect the important effect. We compare the spectra in Fig. 6 with those of the linear systems with different values of the force constant k_d; see Fig. 7. In the low-frequency domain, the lines have the same shape, and we can conclude that the only effect of the quartic nonlinearity in this system is the effective change of the k_d force constant. However, in the high-frequency domain the difference is more noticeable, which can be explained by the influence of the generation and propagation of the third phonon harmonic.

Comparison with simulations of phonon wave packet transmission

The molecular dynamics simulation of phonon wave packet transmission through the atomic defect layer is a commonly used approach in computing phonon transmission coefficients; see, e.g., Refs. [40,54,55]. In our nonlinear lattice-dynamics approach, we also perform the calculation of the wave packet transmission, in which we consider the quasi-1D chain with the embedded nonlinear atomic defect, shown in Fig. 2.

We excite the 1D Gaussian phonon wave packet centered at the frequency ω and wave number k with the spatial width (coherence length) σ. The wave packet is generated by assigning the displacement u_n of the nth atom as

$$u_n = A_{wp} e^{i(kn-wt)} e^{-\frac{n-n_0-v_g t}{4\sigma^2}}, \tag{25}$$

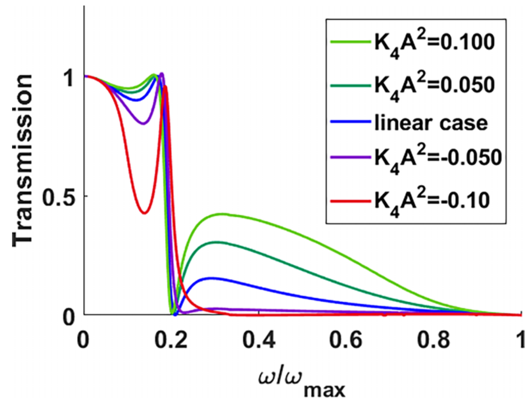

FIG. 6. Spectrum of transmission coefficient in the nonlinear system with weak coupling shown in Fig. 2 with $m_0 = 1$, $m_d = 0$ for different values of quartic nonlinearity. In the legend the lines are indicated from top to bottom.

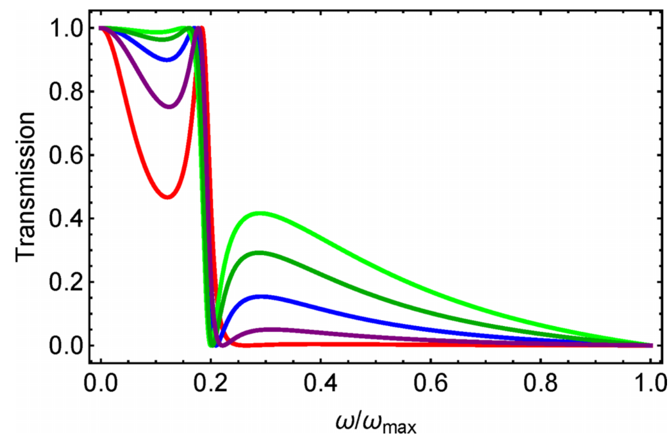

FIG. 7. Spectrum of transmission coefficient through the atomic defect shown in Fig. 2 with $m_0 = 1$, $m_d = 0$ in the linear case for different values of the coefficient k_d for $k_0 = 0.07$: $k_d = 0.49$ (green line); $k_d = 0.39$ (darker green line); $k_d = 0.28$ (blue line); $k_d = 0.174$ (purple line); and $k_d = 0.07$ (red line). The lines are indicated from top to bottom.

where the spatial width is taken to be $\sigma(\omega) = 20\lambda$, $\lambda = \frac{2\pi}{k(\omega)}$ is a wave length at the central frequency, and the phonon group velocity is $v_g = \sqrt{k_{\rm norm}/m}\cos(ka/2)$.

Simulations of the wave packet transmission through the nonlinear atomic defect are held for each value of the frequency ω. The whole chain consists of $2N_{\rm tail} + 2$ particles, where $N_{\rm tail}$ is a number of atoms in the chain fragment on the left and on the right to the structure defect.

The principal question is how to choose the amplitude A_{wp} of the wave packet for the simulation of the transmission of nonlinear wave. We know that the effective nonlinear parameter is $K_4A_{wp}^2$, so the change of A_{wp} changes the nonlinear parameter. In order to compare the transmission coefficients of the plane wave with the given amplitude A and of the phonon wave packet, it is natural to determine A_{wp} from the condition that the lattice deformation energy of the wave packet is equal to the energy of the plane wave on the fragment of the lattice with the length of several coherent lengths σ of the wave packet when this length is less than $2N_{\rm tail} + 2$ lattice periods. In our simulations of phonon wave packets, we consider the transmission through the nonlinear defect of the plane wave with unit amplitude and calculate numerically the amplitude A_{wp} for each value of K_4 and central frequency ω from the condition that the wave packet energy is equal to the energy of the plane wave with unit amplitude for different values of the nonlinear coefficient K_4 on the lattice fragment with the length of 15 or 16 coherence lengths σ, when the latter is proportional in turn to the wave length λ at the central frequency; see Eq. (25). Numerical simulation of the transmission through the nonlinear defect with a given K_4 of phonon wave packet with the amplitude A_{wp}, which is determined on 15 σ length of the lattice fragment, shows a good agreement with the results for the transmission of plane waves with unit amplitude for different values of the nonlinear coefficient K_4 through the 2D array of Ge-like defect atoms in a simple cubic lattice of Si-like atoms shown in Fig. 2; see Fig. 8.

In Figs. 9(a), 9(b) and 9(c), we illustrate the form of the displacement pattern of the aforementioned phonon wave packet before, during, and after, respectively, the transmission through the defect plane of the 2D array of Ge-like defect atoms in a simple cubic lattice of Si-like atoms shown in Fig. 2, for a wave packet reduced central frequency $\omega/\omega_{\rm max} = 0.56$ and $K_4 = -0.005$. In result of partial transmission and reflection, the incident wave packet splits into the two transmitted and reflected wave packets.

For the system with weak coupling, described in Case 3 in Sec. IV, the simulation of wave packet transmission through the nonlinear lattice defect also provides good conformity with the results for the transmission of plane waves with unit amplitude for different values of the nonlinear coefficient K_4 including the high-frequency domain, for the lattice fragment length of 16 σ; see Fig. 10. This is important since one can expect that the nonlinear effects are especially pronounced in the high-frequency domain.

As one can see in Figs. 8 and 10, the minimal value of the transmission coefficient in the antiresonance is nonzero for the

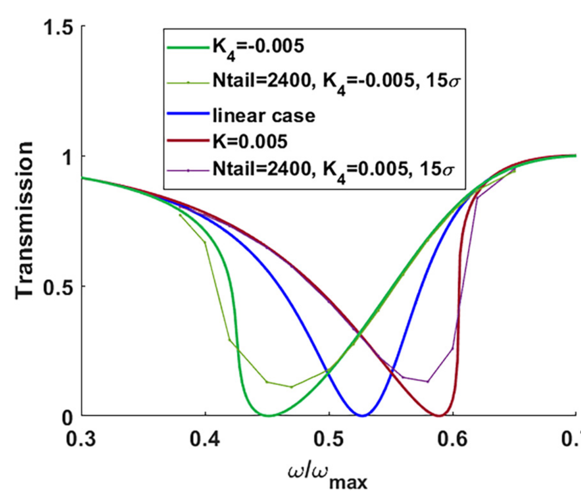

FIG. 8. Comparison of the transmission coefficients of plane waves with unit amplitude (solid lines) and wave packets (thin lines) through the 2D array of Ge-like and Si-like atoms in a simple cubic lattice of Si-like atoms shown in Fig. 2, for positive and negative values of the nonlinear coefficient K_4. In the legend the lines are indicated from left to right.

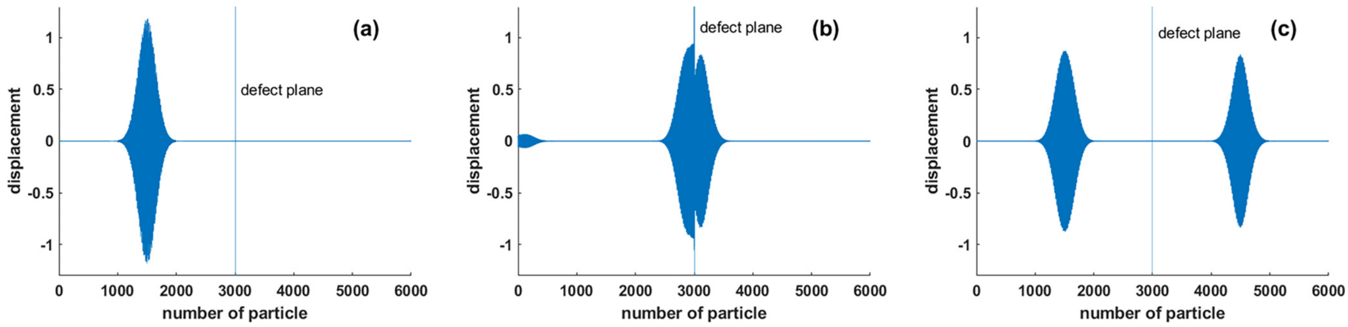

FIG. 9. Form of displacement patterns of phonon wave packet before (a), during (b), and after (c) the transmission through the defect plane of the 2D array of Ge-like and Si-like atoms in a simple cubic lattice of Si-like atoms shown in Fig. 2, for wave packet reduced central frequency $\omega/\omega_{\max} = 0.56$ and $K_4 = -0.005$.

wave packets, which is a consequence of the finite spectral width of the coherent superposition of the plane waves in the packet in contrast to the single frequency of the plane wave; see also Refs. [18,19]. It is worth noting that with the appropriate choice of the lattice fragment length for determining the amplitude of the wave packet A_{wp}, in principle, one can get very good agreement with the analytical prediction for the plane wave transmission, but this is not our goal.

V. INFLUENCE OF CUBIC NONLINEARITY ON PHONON TRANSMISSION

It is well known that the presence of cubic nonlinearity causes the change of the equilibrium bond length; see, e.g., Ref. [53]. To take into account this change, we introduce the additional variables Δ_i for each nonlinear bond; see the Lagrangian (12). Values of these variables are obtained from the full algebraic system for all complex amplitudes; see Appendixes A and B. Estimates for the case of one oscillator with cubic and quartic nonlinearity yield that $\Delta_i \sim -K_3A^2$ supposing that the nonlinearity is relatively weak [53]. We use these estimates to get rid of the negligible terms.

In some systems we can see that the cubic nonlinearity K_3 red shifts the antiresonance frequency independently of the K_3 sign. This effect can be explained by the known red shift of the fundamental frequency of the finite-amplitude oscillations of an oscillator with cubic nonlinearity [53]. For example, with the parameters $k_0 = 1.8$, $k_d = 0.1$, $m_0 = 0$, and $m_d = 1$, in Fig. 11 we can see that for $K_4 = 0$ the antiresonance frequencies experience red shifts. This effect also holds for $K_4A^2 \neq 0$.

In the system with weak coupling where the transmission line has a different shape, the presence of cubic nonlinearity has a similar effect: cubic nonlinearity red shifts the antiresonance frequency independently of the sign of K_3A; see Fig. 12 for the $k_0 = 0.5$, $k_d = 0.2$, $m_0 = 0$, $m_d = 0.5$ parameters set.

But in some systems, an additional narrow resonance emerges. Figure 13(a) shows transmission spectrum for the case $k_0 = 0.5$, $k_d = 0.51$, $m_0 = 0.5$, and $m_d = 1.3$. We see the additional narrow transmission resonance close to the antiresonance frequency, at $\omega \approx 0.5\omega_{\max}$. We relate this effect with the opening of the additional transmission channel for phonon second harmonic in wave paths through the nonlinear defect atoms. Figures 13(b)–13(d) show that the resonance excitation of phonon second harmonic amplitude at and transmission through the nonlinear defect atoms indeed results in a suppression of the amplitude of the phonon fundamental (first) harmonic at the defect and the 0-atoms.

This hypothesis is supported by the study of similar effects in the systems with different parameters. If we change the mass ratio, that is, consider more light defect atoms, the

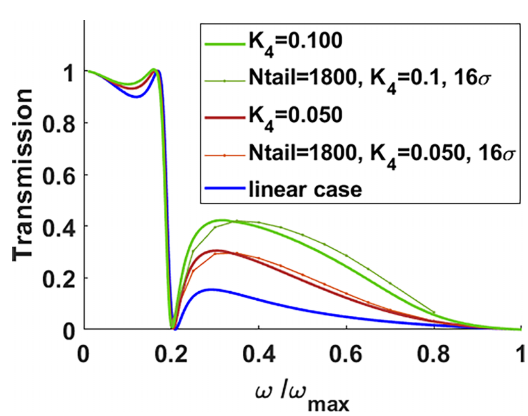

FIG. 10. Comparison of the transmission coefficient of plane waves with unit amplitude (solid lines) and wave packets (thin lines) through the system with weak coupling, described by Case 3 in Sec. IV, for different values of the nonlinear coefficient K_4. In the legend the lines are indicated from top to bottom.

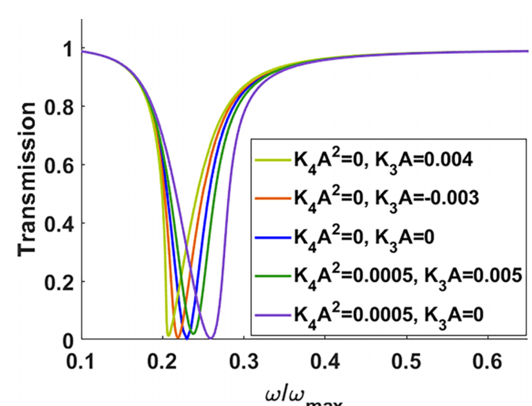

FIG. 11. Antiresonance frequency shift in the case of $k_0 = 1.8$, $k_d = 0.1$, $m_0 = 0.0$, and $m_d = 1$ with both K_3 and K_4 nonlinearities. In the legend the lines are indicated from left to right.

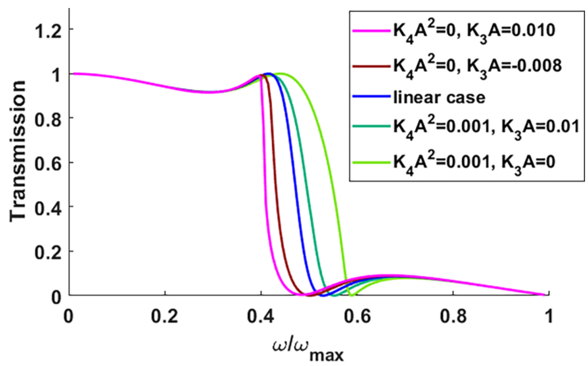

FIG. 12. Antiresonance frequency shift in the case of the system with weak coupling with both K_3 and K_4 nonlinearities. In the legend the lines are indicated from left to right.

position of the narrow resonance remains almost the same, close to $0.5\omega_{\max}$; see Fig. 14.

To illustrate the importance of the opening of the additional transmission channels in this effect, first we consider the linear three-path atomic system, in which an additional path binds the atom with mass m_a through linear force constants k_a with the atoms in the positions -1 and 1 in the model, shown in Fig. 2, in parallel with the paths through the defect atom with mass $m_d = 1.3m$ and linear force constants $k_d = 0.51k_{\text{norm}}$ and through the 0-atom with mass $m_0 = 0.5m$ and linear force constants $k_0 = 0.5k_{\text{norm}}$; see Fig. 15. The additional path in this model is considered to be very weak because it is assumed that only a small fraction of defect atoms in the array are bypassed with such paths, which in turn models the relatively weak amplitude of phonon second harmonic and the resulting spectral narrowness of transmission resonance in the considered nonlinear atomic-scale system. Namely, we consider as an example the case when the additional path bypasses one defect atom in the area of 12×12 atoms in the 2D array. This corresponds to the case of the $k_a = k_{\text{norm}}/144 = 0.0069k_{\text{norm}}$ effective force constant connecting with the matrix the atoms with mass $m_a = 0.0069 \times 1.8m$, which have a resonance frequency that coincides with the antiresonance frequency, close to $0.5\omega_{\max}$, in the model shown in Fig. 15. Figure 16(a) shows the appearance of a narrow resonance in a transmission through the sparse 2D array of Ge-like defect atoms in a simple cubic lattice of Si-like atoms with the additional weak linear transmission channel; Figs. 16(b) and 16(c) show the sharp antiresonance suppression of the displacements of the d- and 0-atoms that is accompanied by the resonance displacement enhancement of the a-atoms, shown in Fig. 16(d), in the additional weak transmission channel. The comparison of Figs. 13, 14, and 16 confirms that the opening of the additional transmission channel for the phonon second harmonic through the nonlinear defect atoms is the origin of the narrow transmission resonance caused by cubic nonlinearity.

It is worth noting in this connection that the total transmission in the linear systems close to the frequency $0.7\omega_{\max}$, such as is shown in Figs. 4, 5, 13(a), and 16(a), is also accompanied by the complete suppression of the d-atom oscillation amplitude, with $u_d = 0$ at this frequency, as one can see in Figs. 13(b) and 16(b). This property provides further evidence that the narrow resonance of the transmission enhancement, shown in Figs. 13(a) and 14, is related with the suppression of the d-atom oscillation amplitude in the fundamental harmonic, which in turn is caused by resonance excitation of and interaction with the phonon second harmonic in the nonlinear system, as Fig. 13(d) confirms. Below we will discuss the origin of the value close to $0.5\omega_{\max}$ of the frequency of the transmission resonance caused by phonon second harmonic.

To model the appearance of the additional narrow transmission resonance in the nonlinear system, we consider the atomic system, which is a chain with the defect shown in Fig. 1(b), but we divide the nonlinear path into two nonlinear paths with close linear and nonlinear phononic parameters, when $k_0 \approx k_d$ and $m_0 \approx m_d$; see Fig. 17. In this case we should take into account that four equilibrium bond lengths effectively change, and the corresponding FPU Lagrangian with cubic nonlinearity reads as

$$
\begin{aligned}
\mathcal{L} = {} & \sum_{i=-\infty}^{-1} \frac{m\dot{u}_i^2}{2} + \frac{m_0\dot{u}_0^2}{2} + \frac{m_d\dot{u}_d^2}{2} + \sum_{i=1}^{\infty} \frac{m\dot{u}_i^2}{2} \\
& - \Bigg(\frac{k_0(u_0 - u_{-1} - \Delta_{20})^2}{2} + \frac{K_{30}(u_0 - u_{-1} - \Delta_{20})^3}{3} \\
& + \frac{k_0(u_1 - u_0 - \Delta_{10})^2}{2} + \frac{K_{30}(u_1 - u_0 - \Delta_{10})^3}{3} \\
& + \frac{k_d(u_d - u_{-1} - \Delta_{2d})^2}{2} + \frac{K_{3d}(u_d - u_{-1} - \Delta_{2d})^3}{3} \\
& + \frac{k_d(u_1 - u_d - \Delta_{1d})^2}{2} + \frac{K_{3d}(u_1 - u_d - \Delta_{1d})^3}{3} \\
& + \sum_{i \neq -1,0} \frac{k_{\text{norm}}(u_{i+1} - u_i)^2}{2} + \frac{C(u_1 - u_{-1})^2}{2} \Bigg).
\end{aligned} \tag{26}
$$

Figure 18 shows the appearance of the narrow resonances induced by the asymmetry in linear and/or nonlinear wave paths in the system shown in Fig. 17. One can see that the induced narrow resonances occur at different frequencies in asymmetric linear and in asymmetric nonlinear systems. Figure 18 clearly shows that the narrow, the Fano-like, transmission antiresonances with asymmetric line shapes are caused by the presence of the two *weakly split* wave paths, either linear or nonlinear, through the embedded atomic defect shown in Fig. 17. At the same time, the relatively broad *background antiresonances*, shown in Figs. 13, 14, 16, and 18, are related with the transmission through the two very different wave paths, shown in Figs. 1(b), 2, 15, and 17.

Spectral position of the additional narrow transmission resonances or antiresonances close to $0.5\omega_{\max}$ in Figs. 13, 14, and 18 can be explained in the following way. The second harmonic of the resonance frequency is close to $\omega_{\max}$ when the nearest lattice neighbors oscillate out of phase, while the same particles oscillate in phase with the frequency close to $0.5\omega_{\max}$. If applied to the -1-st and defect atoms in the atomic defect shown in Fig. 2, this can result in the suppression of the oscillation amplitude of the d-atom, for the given amplitude of the -1-st atom provided by the incident lattice wave. The suppression of the d-atom oscillation amplitude effectively blocks the wave path for the fundamental harmonic

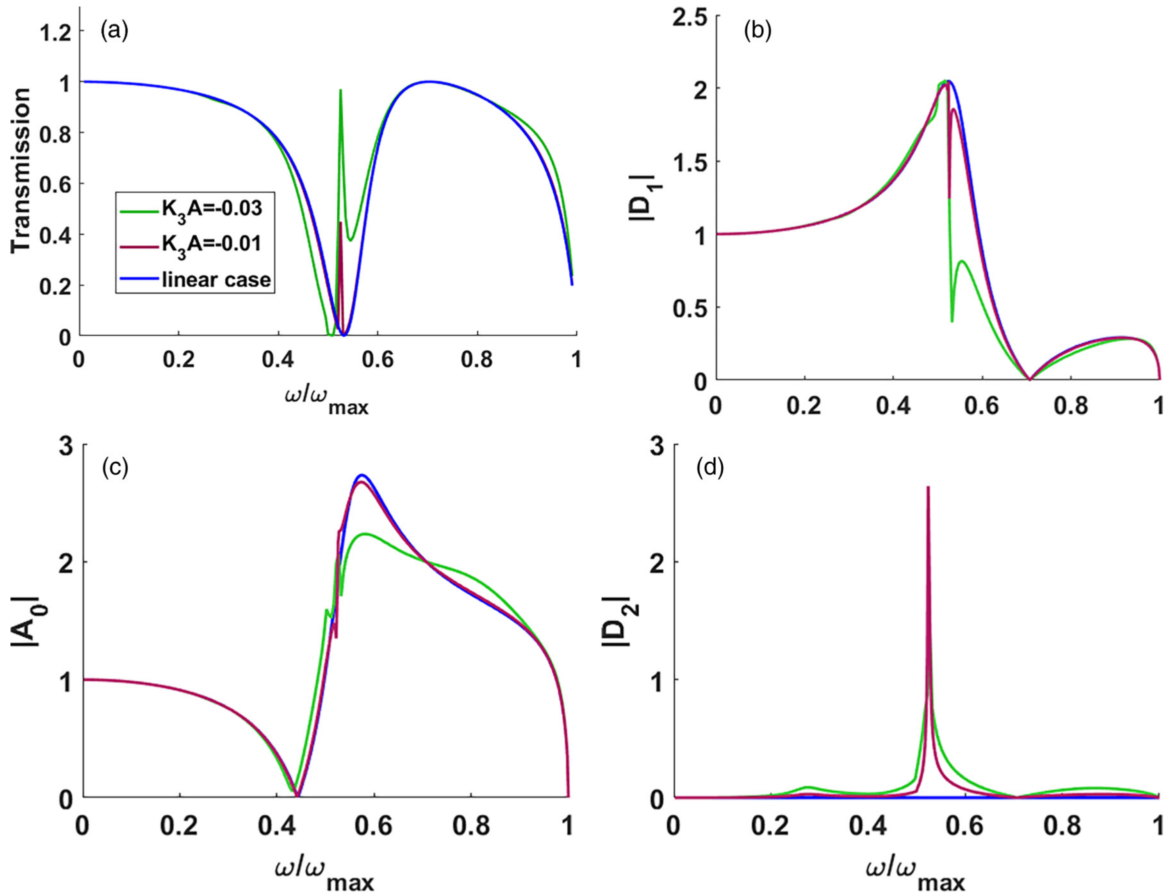

FIG. 13. (a) Narrow transmission resonance due to the cubic nonlinearity in a sparse 2D array of Ge-like nonlinear defect atoms in a simple cubic lattice of Si-like atoms, shown in Fig. 2. Spectrum of the displacement amplitudes of the first harmonic of the defect atoms $|D_1|$ (b), of the 0-atoms $|A_0|$ (c), and of the second harmonic of the defect atoms $|D_2|$ (d). Parameter set: $k_0 = 0.5$, $k_d = 0.51$, $m_0 = 0.5$, $m_d = 1.3$.

through the d-atom. The second-harmonic wave propagation through the path with the 0-atom [see Eq. (18)] blocks the wave path for the fundamental harmonic through the 0-atom as well; see Fig. 13(c). Blocking the wave paths for the fundamental harmonic through the d- and 0-atoms suppresses the destructive-interference antiresonance and results in the appearance of the additional narrow nonlinearity-induced transmission peak, shown in Figs. 13, 14, and 18(b). If applied to the defect and 1-st atoms in the atomic defect shown in Fig. 2, this can result in the suppression of the oscillation amplitude of the 1-st atom and the appearance of the additional narrow nonlinearity-induced antiresonance, shown in Figs. 14 and 18(a).

The absence of the additional narrow transmission resonance or antiresonance close to $0.5\omega_{\max}$ in the spectra shown in Figs. 11 and 12 can be related to the absence of the atom (with finite mass) in one of the wave paths in the corresponding atomic systems. Figures 11 and 12 present the

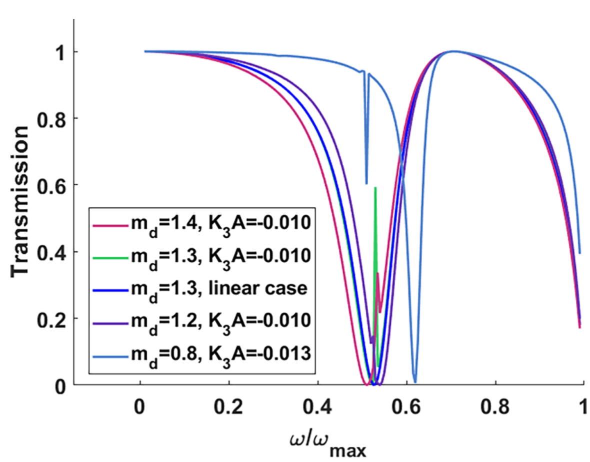

FIG. 14. Narrow resonance due to the cubic nonlinearity in a matrix with different masses of nonlinear defect atoms. In the legend the lines are indicated from left to right.

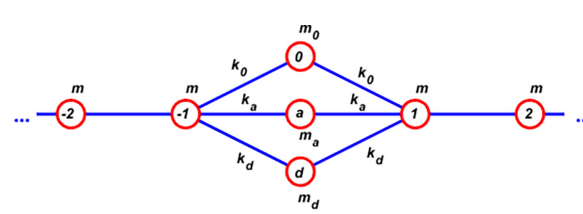

FIG. 15. Quasi-1D model of atomic system with three different linear wave paths, two strong, through atoms 0 and d, and one weak, through atom a.

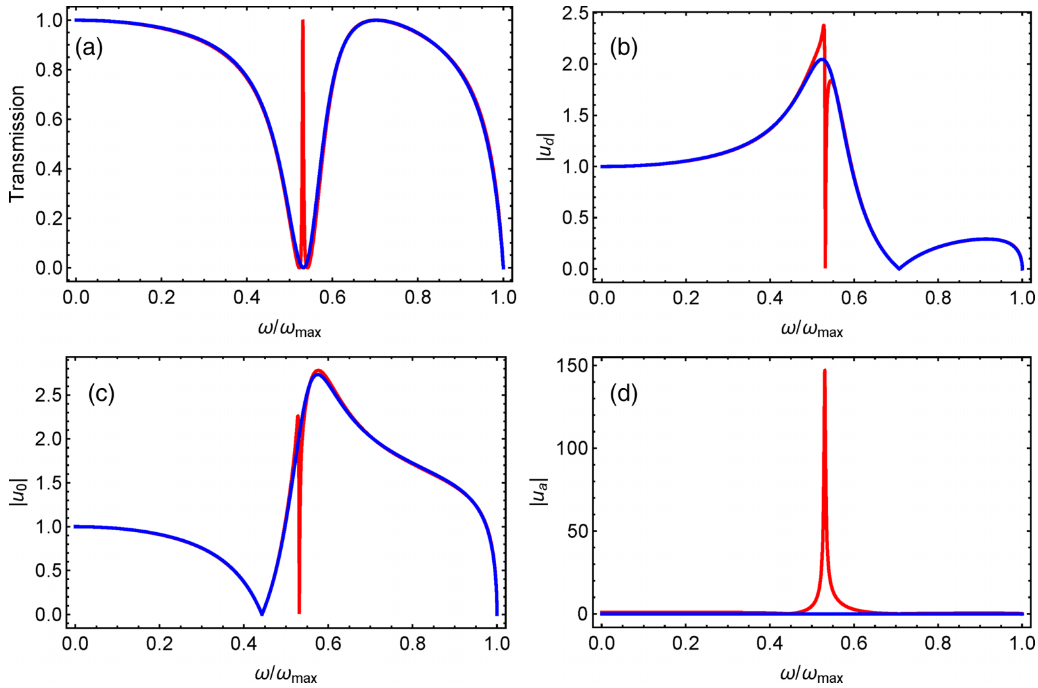

FIG. 16. (a) Narrow transmission resonance in the linear three-path system shown in Fig. 15 with the additional weak channel through a sparse 2D array of Ge-like defect atoms in a simple cubic lattice of Si-like atoms. Spectrum of the displacement amplitudes of the defect atoms (b), the 0-atoms (c), and the a-atoms in the additional channel (d). Red and blue lines show, respectively, the spectra of the atomic system with and without the additional transmission channel. Parameter set: $k_0 = 0.5$, $k_d = 0.51$, $k_a = 0.0069$, $m_0 = 0.5$, $m_d = 1.3$, $m_a = 0.0069 \times 1.8$.

transmission spectra through the nonlinear atomic systems of the type, shown in Fig. 1(b), with $m_0 = 0$ that is equivalent to the direct bond between the -1-st and 1-st atoms with the $k_0/2$ force constant. Because of the absence of the atom in the channel, the suppression of the d-atom oscillation amplitude in the nonlinear channel does not provide the blocking of the wave path through the direct bond in another channel such as the blocking of the channel through the atom, shown in Figs. 13(c) and 16(c). This in turn does not induce the additional narrow transmission resonance or antiresonance, such as shown in Figs. 13(a), 14, and 16(a). The same arguments can be applied to the system shown in Fig. 17 with the transmission spectra shown in Fig. 18. This system with identical paths through the d- and 0-atoms belongs to the nonlinear atomic system of the type, shown in Fig. 1(b), which does not produce the additional narrow transmission resonance or antiresonance close to $0.5\omega_{\max}$ that emerges only in the presence of the *asymmetry of two nonlinear wave paths*, through the d- and 0-atoms as Figs. 18(a) and 18(b) show.

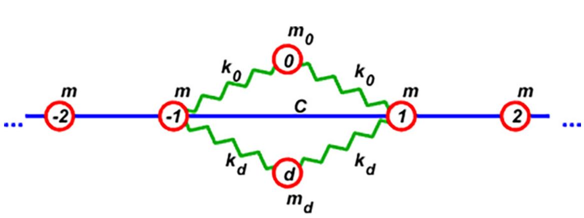

FIG. 17. Quasi-1D model of atomic system with three different wave paths, two weakly split nonlinear and a linear.

VI. TOPOLOGICALLY DIFFERENT EMBEDDED NONLINEAR ATOMIC SYSTEM

Now we consider antiresonances in topologically different embedded nonlinear atomic system, which we relate to the structure of the 2D two-path planar defect in a diamond-like cubic lattice with two atoms per unit cell; see Fig. 19. Such two-monolayer embedded atomic defect we consider as a realistic model for the 2D array of defects, formed by heavy Ge atoms embedded in diamond-like cubic lattice of more light Si atoms (see Ref. [21]), and here we analyze the effects of quartic nonlinearity on the transmission through the array of such defects.

We describe the system by the following FPU Lagrangian with quartic nonlinearity:

$$\begin{aligned}\mathcal{L} = &\sum_{i=-\infty}^{-1}\frac{m\dot{u}_i^2}{2} + \frac{m_0\dot{u}_{0A}^2}{2} + \frac{m_0\dot{u}_{0B}^2}{2} + \frac{m_0\dot{u}_{dB}^2}{2} + \frac{m_d\dot{u}_{dA}^2}{2}\\ &+\sum_{i=1}^{\infty}\frac{m\dot{u}_i^2}{2} - \left(\sum_{i\neq 0,-1}\frac{k_{\text{norm}}(u_i-u_{i-1})^2}{2} + \frac{k_0(u_{0A}-u_{-1})^2}{2}\right.\\ &+\frac{k_0(u_{0B}-u_{0A})^2}{2} + \frac{k_0(u_{0B}-u_1)^2}{2} + \frac{k_d(u_{dA}-u_{-1})^2}{2}\\ &+\frac{K_4(u_{dA}-u_{-1})^4}{4} + \frac{k_d(u_{dB}-u_{dA})^2}{2}\\ &\left.+\frac{K_4(u_{dB}-u_{dA})^4}{4} + \frac{k_d(u_1-u_{dB})^2}{2} + \frac{K_4(u_1-u_{dB})^4}{4}\right).\end{aligned} \tag{27}$$

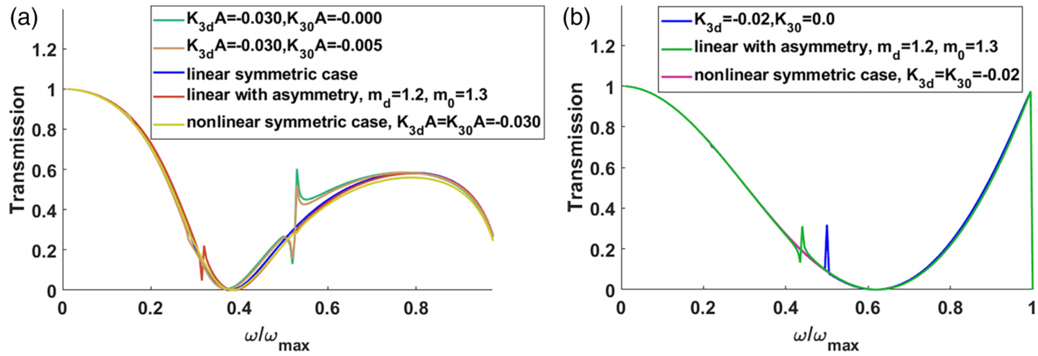

FIG. 18. Narrow resonances due to the asymmetry in linear (atom masses $m_0 \neq m_d$) and nonlinear (coefficients $K_{30} \neq K_{3d}$) wave paths in the transmission spectrum through the system shown in Fig. 16. Parameter set: $m_0 = 1.3$, $m_d = 1.2$ for the linear asymmetry case and $m_0 = 1.3$, $m_d = 1.3$ in other cases, $C = 0.50$ with $k_0 = k_d = 0.25$ in (a) and with $k_0 = k_d = 0.5$ in (b). In the legends the lines are indicated from top to bottom.

We use the same approach to solve the equations of motion, which follow from the Lagrangian (27) and obtain the transmission spectrum. Two antiresonances are present in the transmission spectrum through such array of defects, with $m_0 = 0.5m$, $m_d = 1.3m$, $k_0 = k_d = 0.5k_{\text{norm}}$ (see Fig. 20), which are related with the two-monolayer structure of the 2D atomic defect [21]. Figure 20 also shows that spectral positions of the two antiresonances are shifted in the nonlinear case and spectral line shape can be strongly affected by moderate nonlinear coefficient K_4, especially positive. Lattice wave transmission close to the antiresonances becomes bistable for the higher quartic nonlinearity similar to the transmission bistability described in optical chain with a quartic nonlinear defect [8]. As was emphasized above, in the linear case the two transmission antiresonances of phonons in the two-path two-monolayer atomic defect shown in Fig. 20 have the same destructive-interference origin as the two transmission antiresonances of photons in the two-path double-layer stereometamaterials, which were observed in Ref. [27], despite the fact that the damping of local nanoplasmonic resonances in periodic nanostructures weakens the photon transmission dips.

VII. CONCLUSIONS

In summary, we present the theoretical studies of the effects of nonlinearity on the two-path phonon transmittance through the 2D arrays of atomic defects in a lattice. We demonstrate the appearance of transmission antiresonance (transmission node) in the two-path systems with the few-particle nanostructures, which allow one to model both linear and nonlinear phonon antiresonances. The universality of destructive-interference origin of transmission antiresonances of waves of different nature, such as phonons, photons, and electrons, in two-path nanostructures and metamaterials is emphasized. The full system of nonlinear algebraic equations for the amplitudes of the transmission through and reflection at nonlinear two-path atomic defects with an account for the generation of second and third harmonics is derived in the proposed nonlinear lattice-dynamics approach. The system of nonlinear algebraic equations is further solved numerically. We show that the quartic interatomic nonlinearity in the atomic defect shifts the antiresonance frequency in the direction, determined by the sign of the nonlinear coefficient. The quartic nonlinearity also enhances in general the transmission of high-frequency phonons due to third harmonic generation and propagation. The effects of the quartic nonlinearity on phonon transmission and propagation are described for the two-path atomic defects with different topology. We also model the transmission through the nonlinear two-path atomic defects by launching the phonon wave packet, for which the proper amplitude normalization is proposed and implemented. We show that the cubic interatomic nonlinearity in the atomic defect red shifts in general the antiresonance frequency independently of the sign of the nonlinear coefficient, and the equilibrium interatomic distances (bond lengths) in

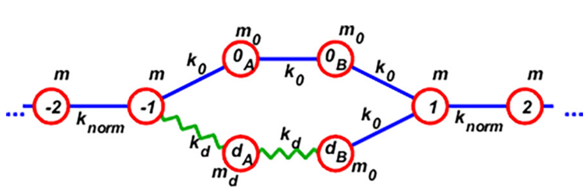

FIG. 19. Quasi-1D model of lattice system with two-monolayer atomic defect.

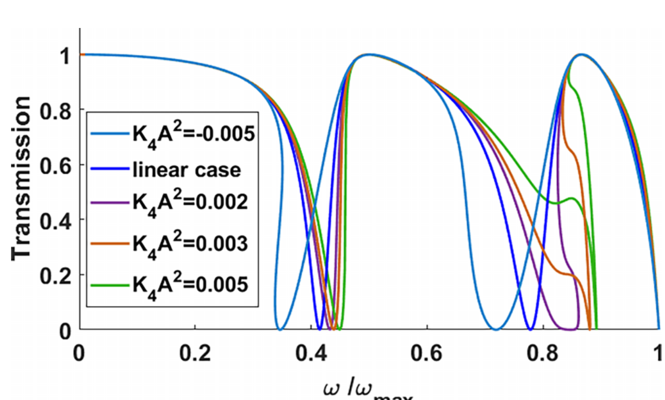

FIG. 20. Transmission spectrum through the two-monolayer atomic defect, shown in Fig. 19, with $m_0 = 0.5m$, $m_d = 1.3m$, $k_0 = k_d = 0.5k_{\text{norm}}$, for different amplitudes of the incident plane wave. In the legend the lines are indicated from left to right.

the atomic defect are changed by the incident phonon due to cubic interatomic nonlinearity.

In the systems with the cubic nonlinearity, the new narrow transmission resonance on the background of a broad antiresonance can appear, which we relate to the opening of the additional transmission channel for phonon second harmonic through the embedded nonlinear atomic defects. Conditions of the existence of the new nonlinear transmission resonance are determined and demonstrated for different embedded two-path nonlinear atomic systems. A two-dimensional array of embedded three-path atomic defects with an additional weak transmission channel, in which a linear analog of the nonlinear narrow transmission resonance on the background of a broad antiresonance is realized, is also proposed and modeled. The linear analog helps to understand the origin of the new nonlinear transmission resonance.

The presented results contribute to the better understanding and detailed modeling of the interplay between the interference and nonlinearity in phonon propagation through and scattering in 2D arrays of two-path anharmonic atomic defects with different topology.

ACKNOWLEDGMENTS

Yu.A.K. is grateful to Masahiro Nomura and Sebastian Volz for useful discussions. This work was funded at the initial stage in part by RFBR and JSPS (Project No. 19-52-50030) for the rigorous formulation of the problem. This work was supported by the Program of Fundamental Researches of the Russian Academy of Sciences (Project No. FFZE-2022-0009, State Registration No. 122040500069-7). Yu.A.K. acknowledges support from the CREST Japan Science and Technology Agency (Grant No. JPMJCR19I1) for the lattice dynamics calculations and results analyzing.

APPENDIX A: ANALYTICAL TECHNIQUE OF TRANSMISSION COEFFICIENT CALCULATION

We have six equations of motion for $u_{-2}, \dots, u_2, u_d$ displacements, which follow from the Lagrangian (12). Substituting the expressions (13)–(14) and (18)–(21) into these equations and equating the coefficients in front of $e^0 = 1$, $e^{-i\omega t}$, $e^{-2i\omega t}$, and $e^{-3i\omega t}$, we get 20 algebraic equations for 20 complex amplitudes. For example, the equation of motion for the defect atom is the following:

$$\begin{aligned} m_d\ddot{u}_d - k_d(u_1 - u_d - \Delta_1) - K_3(u_1 - u_d - \Delta_1)^2 - K_4(u_1 - u_d - \Delta_1)^3 \\ + k_d(u_d - u_{-1} - \Delta_2) + K_3(u_d - u_{-1} - \Delta_2)^2 + K_4(u_d - u_{-1} - \Delta_2)^3 = 0. \end{aligned} \tag{A1}$$

Since all the coefficients A_0, D_1, etc., are normalized, we also introduce the normalized bond length changes $\delta_i = \Delta_i/A$. Substituting the expression (21) for u_d, we get

$$\begin{aligned} & m_d(-\omega^2 D_1 e^{-i\omega t} - 4\omega^2 D_2 e^{-2i\omega t} - 9\omega^2 D_3 e^{-3i\omega t}) + k_d(\delta_1 - \delta_2) + k_d(2D_1 - A_{-1} - t_1)e^{-i\omega t} \\ & + k_d(2D_2 - r_{2,-1} - t_{2,1})e^{-2i\omega t} + k_d(2D_3 - r_{3,-1} - t_{3,1})e^{-3i\omega t} \\ & - K_3A[\delta_1 + (D_1 - t_1)e^{-i\omega t} + (D_2 - t_{2,1})e^{-2i\omega t} + (D_3 - t_{3,1})e^{-3i\omega t} + \text{c.c.}]^2 \\ & \times K_3A[-\delta_2 + (D_1 - A_{-1})e^{-i\omega t} + (D_2 - r_{2,-1})e^{-2i\omega t} + (D_3 - r_{3,-1})e^{-3i\omega t} + \text{c.c.}]^2 \\ & \times K_4A^2[\delta_1 + (D_1 - t_1)e^{-i\omega t} + (D_2 - t_{2,1})e^{-2i\omega t} + (D_3 - t_{3,1})e^{-3i\omega t} + \text{c.c.}]^3 \\ & \times K_4A^2[-\delta_2 + (D_1 - A_{-1})e^{-i\omega t} + (D_2 - r_{2,-1})e^{-2i\omega t} + (D_3 - r_{3,-1})e^{-3i\omega t} +)]^3 = 0. \end{aligned} \tag{A2}$$

This equation yields four algebraic equations (the coefficients in front of $e^0 = 1$, $e^{-i\omega t}$, $e^{-2i\omega t}$, and $e^{-3i\omega t}$):

$$k_d(\delta_1 - \delta_2) + K_3A\left(\delta_2^2 - \delta_1^2 - 2|D_1 - t_1|^2 + 2|D_1 - A_{-1}|^2\right) + K_4A^2\left(\delta_1^3 - \delta_2^3\right) = 0, \tag{A3}$$

$$\begin{aligned} & m_d(-D_1\omega^2) + k_d(2D_1 - A_{-1} - t_1) - K_3A[2\delta_1(D_1 - t_1) + 2(D_2 - t_{2,1})(D_1{}^* - t_1{}^*)] \\ & + K_3A[-2\delta_2(D_1 - A_{-1}) + 2(D_2 - r_{2,-1})(D_1{}^* - A_{-1}{}^*)] + K_4A^2[3(D_1 - A_{-1})^2(D_1{}^* - A_{-1}{}^*) + 3(D_1{}^* - A_{-1}{}^*)^2(D_3 - r_{3,-1}) \\ & + 3\delta_2{}^2(D_1 - A_{-1}) - 6\delta_2(D_2 - r_{2,-1})(D_1{}^* - A_{-1}{}^*)] + K_4A^2[3(D_1 - t_1)^2(D_1{}^* - t_1{}^*) + 3(D_1{}^* - t_1{}^*)^2(D_3 - t_{3,1}) \\ & + 3\delta_1{}^2(D_1 - t_1) + 6\delta_1(D_2 - t_{2,1})(D_1{}^* - t_1{}^*)] = 0, \end{aligned} \tag{A4}$$

and the corresponding equation for $e^{-2i\omega t}$ and $e^{-3i\omega t}$.

It is desirable to simplify the obtained algebraic system. In the brackets with the coefficient K_4A^2, the first term is of the 0-th order, and the second one is of the 1-st order. So we neglect the terms $3(D_1{}^* - A_{-1}{}^*)^2(D_3 - r_{3,-1})$ and $3(D_1{}^* - t_1{}^*)^2(D_3 - t_{3,1})$ in Eq. (A4). Also we suppose that δ_1 and δ_2 are of the same order of smallness, so we neglect the terms that are smaller than other terms. The same simplification is made in other equations. In result, we get the following system:

$$\begin{aligned} & m_d(-D_1\omega^2) + k_d(2D_1 - A_{-1} - t_1) - K_3A[2\delta_1(D_1 - t_1) + 2(D_2 - t_{2,1})(D_1{}^* - t_1{}^*)] + K_3A[-2\delta_2(D_1 - A_{-1}) \\ & + 2(D_2 - r_{2,-1})(D_1{}^* - A_{-1}{}^*)] + K_4A^2[3(D_1 - A_{-1})^2(D_1{}^* - A_{-1}{}^*) + 3(D_1 - t_1)^2(D_1{}^* - t_1{}^*)] = 0, \end{aligned} \tag{A5}$$

$$m_d(-4\omega^2 D_2) + k_d(2D_2 - r_{2,-1} - t_{2,1}) + K_3A[-(D_1 - t_1)^2 + (D_1 - A_{-1})^2] = 0, \tag{A6}$$

$$m_d(-9\omega^2 D_3) + k_d(2D_3 - r_{3,-1} - t_{3,1}) + K_3A[-2(D_1 - t_1)(D_2 - t_{2,1}) + 2(D_1 - A_{-1})(D_2 - r_{2,-1})] + K_4A^2[(D_1 - A_{-1})^3 + (D_1 - t_1)^3] = 0, \tag{A7}$$

$$m(-t_1\omega^2) + k_0(t_1 - A_0) + k_{\rm norm}(t_1 - te^{2ika}) + k_d(t_1 - D_1) + K_3[-2\delta_1(t_1 - D_1) + 2(t_{2,1} - D_2)(t_1{}^* - D_1{}^*)] + K_4A^2[3(t_1 - D_1)^2(t_1^* - D_1^*)] = 0, \tag{A8}$$

$$m(-4t_{2,1}\omega^2) + k_0(t_{2,1} - t_{2,0}) + k_{\rm norm}(t_{2,1} - t_2e^{2ik_2a}) + k_d(t_{2,1} - D_2) + K_3A[(t_1 - D_1)^2] = 0, \tag{A9}$$

$$m(-9t_{3,1}\omega^2) + k_0(t_{3,1} - t_{3,0}) + k_{\rm norm}(t_{3,1} - t_3e^{2ik_3a}) + k_d(t_{3,1} - D_3) + K_3A[2(t_1 - D_1)(t_{2,1} - D_2)] + K_4A^2[(t_1 - D_1)^3] = 0, \tag{A10}$$

$$m(-A_{-1}\omega^2) + k_0(A_{-1} - A_0) + k_{\rm norm}(A_{-1} - e^{-2ika} - re^{2ika}) + k_d(A_{-1} - D_1) - K_3A(2\delta_2(A_{-1} - D_1) + 2(r_{2,-1} - D_2)[A_{-1}{}^* - D_1{}^*)] + K_4A^2[3(A_{-1} - D_1)^2(A_{-1}^* - D_1^*)] = 0, \tag{A11}$$

$$m(-4\omega^2 r_{2,-1}) + k_0(r_{2,-1} - t_{2,0}) + k_{\rm norm}(r_{2,-1} - r_2e^{2ik_2a}) + k_d(r_{2,-1} - D_2) + K_3A[(A_{-1} - D_1)^2] = 0, \tag{A12}$$

$$m(-9r_{3,-1}\omega^2) + k_0(r_{3,-1} - t_{3,0}) + k_{\rm norm}(r_{3,-1} - r_3e^{2ik_3a}) + k_d(r_{3,-1} - D_3) + K_3A[2(A_{-1} - D_1)(r_{2,-1} - D_2)] + K_4A^2[(A_{-1} - D_1)^3] = 0, \tag{A13}$$

$$m_0(-\omega^2)A_0 + k_0(2A_0 - A_{-1} - t_1) = 0, \tag{A14}$$

$$m_0(-4\omega^2)t_{2,0} + k_0(2t_{2,0} - r_{2,-1} - t_{2,1}) = 0, \tag{A15}$$

$$m_0(-9\omega^2)t_{3,0} + k_0(2t_{3,0} - t_{3,1} - r_{3,-1}) = 0, \tag{A16}$$

$$m(-\omega^2)te^{2ika} + k_{\rm norm}(2te^{2ika} - t_1 - te^{3ika}) = 0, \tag{A17}$$

$$m(-4\omega^2)t_2e^{2ik_2a} + k_{\rm norm}(2t_2e^{2ik_2a} - t_{2,1} - t_2e^{3ik_2a}) = 0, \tag{A18}$$

$$m(-9\omega^2)t_3e^{2ik_3a} + k_{\rm norm}(2t_3e^{2ik_3a} - t_{3,1} - t_3e^{3ik_3a}) = 0, \tag{A19}$$

$$m(-\omega^2)(e^{-2ika} + re^{2ika}) + k_{\rm norm}(2e^{-2ika} + 2re^{2ika} - e^{-3ika} - re^{3ika} - A_{-1}) = 0, \tag{A20}$$

$$m(-4\omega^2)r_2e^{2ik_2a} + k(2r_2e^{2ik_2a} - r_{2,-1} - r_2e^{3ik_2a}) = 0. \tag{A21}$$

$$m(-9\omega^2)r_3e^{2ik_3a} + k(2r_3e^{2ik_3a} - r_{3,-1} - r_3e^{3ik_3a}) = 0. \tag{A22}$$

$$k_d(\delta_1 - \delta_2) + K_3A\left(\delta_2^2 - \delta_1^2 - 2|D_1 - t_1|^2 + 2|D_1 - A_{-1}|^2\right) + K_4A^2\left(\delta_1^3 - \delta_2^3\right) = 0, \tag{A23}$$

$$-k_d\delta_1 + K_3A\left(\delta_1^2 + 2|t_1 - D_1|^2\right) - K_4A^2\delta_1^3 = 0, \tag{A24}$$

$$k_d\delta_2 - K_3A\left(\delta_2^2 + 2|D_1 - A_{-1}|^2\right) + K_4A^2\delta_2^3 = 0. \tag{A25}$$

We have 21 equations, Eqs. (A5)–(A25), but the last three equations yield zero in the l.h.s. in a sum, so we have effectively 20 independent complex algebraic equations for 20 independent complex variables.

For the system with the two-monolayer defect, shown in Fig. 19, the algebraic system of equations will be different but can also be obtained from the Lagrangian (27) within the same approach.

APPENDIX B: EQUATIONS FOR THE SYSTEM WITH TWO NONLINEAR WAVE PATHS

If we consider the system with two nonlinear wave paths, described by the Lagrangian (26), we should take into account that equilibrium bond lengths are changing in both nonlinear paths, that is, introduce the additional variables δ_{10}, δ_{20}, δ_{1d}, δ_{2d}. We also take into account a linear bond C between the -1-st and 1-st atoms. In this case, we do not take into account the K_4

nonlinearity. The algebraic system in this case is the following:

$$\begin{aligned} &m_d(-D_1\omega^2) + k_d(2D_1 - A_{-1} - t_1) - K_{3d}A[2\delta_{1d}(D_1 - t_1) + 2(D_2 - t_{2,1})(D_1{}^* - t_1{}^*)] \\ &\quad + K_{3d}A[-2\delta_{2d}(D_1 - A_{-1}) + 2(D_2 - r_{2,-1})(D_1{}^* - A_{-1}{}^*)], \end{aligned} \tag{B1}$$

$$m_d(-4\omega^2 D_2) + k_d(2D_2 - r_{2,-1} - t_{2,1}) + K_{3d}A[-(D_1 - t_1)^2 + (D_1 - A_{-1})^2] = 0, \tag{B2}$$

$$m_d(-9\omega^2 D_3) + k_d(2D_3 - r_{3,-1} - t_{3,1}) + K_{3d}A[-2(D_1 - t_1)(D_2 - t_{2,1}) + 2(D_1 - A_{-1})(D_2 - r_{2,-1})] = 0, \tag{B3}$$

$$\begin{aligned} &m(-t_1\omega^2) + k_0(t_1 - A_0) + k_{\text{norm}}(t_1 - te^{2ika}) + k_d(t_1 - D_1) + C(t_1 - A_{-1}) + K_{3d}A[-2\delta_{1d}(t_1 - D_1) + 2(t_{2,1} - D_2)(t_1{}^* - D_1{}^*)] \\ &\quad - K_{30}A[-2\delta_{10}(t_1 - A_0) + 2(t_{2,1} - t_{2,0})(t_1^* - A_0^*)] = 0, \end{aligned} \tag{B4}$$

$$m(-4t_{2,1}\omega^2) + k_0(t_{2,1} - t_{2,0}) + k_{\text{norm}}(t_{2,1} - t_2e^{2ik_2a}) + k_d(t_{2,1} - D_2) + C(t_{2,1} - r_{2,-1}) + K_{3d}A(t_1 - D_1)^2 - K_{30}A(t_1 - A_0)^2 = 0, \tag{B5}$$

$$\begin{aligned} &m(-9t_{3,1}\omega^2) + k_0(t_{3,1} - t_{3,0}) + k_{\text{norm}}(t_{3,1} - t_3e^{2ik_3a}) + k_d(t_{3,1} - D_3) + C(t_{3,1} - r_{3,-1}) + K_{3d}A[2(t_1 - D_1)(t_{2,1} - D_2)] \\ &\quad - K_{30}A[2(t_1 - A_0)(t_{2,1} - t_{2,0})] = 0, \end{aligned} \tag{B6}$$

$$\begin{aligned} &m(-A_{-1}\omega^2) + k_0(A_{-1} - A_0) + k_{\text{norm}}(A_{-1} - e^{-2ika} - re^{2ika}) + k_d(A_{-1} - D_1) \\ &\quad + C(A_{-1} - t_1) - K_{3d}A[2\delta_{2d}(A_{-1} - D_1) + 2(r_{2,-1} - D_2)(A_{-1}{}^* - D_1{}^*)] \\ &\quad + K_{30}A[2\delta_{20}(A_{-1} - A_0) + 2(r_{2,-1} - t_{2,0})(A_{-1}{}^* - A_0{}^*)] = 0, \end{aligned} \tag{B7}$$

$$\begin{aligned} &m(-4\omega^2 r_{2,-1}) + k_0(r_{2,-1} - t_{2,0}) + k_{\text{norm}}(r_{2,-1} - r_2e^{2ik_2a}) + k_d(r_{2,-1} - D_2) \\ &\quad + C(r_{2,-1} - t_{2,1}) + K_{3d}A(A_{-1} - D_1)^2 - K_{30}A(A_{-1} - A_0)^2 = 0, \end{aligned} \tag{B8}$$

$$\begin{aligned} &m(-9r_{3,-1}\omega^2) + k_0(r_{3,-1} - t_{3,0}) + k_{\text{norm}}(r_{3,-1} - r_3e^{2ik_3a}) + k_d(r_{3,-1} - D_3) + C(r_{3,-1} - t_{3,1}) \\ &\quad + K_{3d}A[2(A_{-1} - D_1)(r_{2,-1} - D_2)] - K_{30}A[2(A_{-1} - A_0)(r_{2,-1} - t_{2,0})] = 0, \end{aligned} \tag{B9}$$

$$\begin{aligned} &m_0(-\omega^2)A_0 + k_0(2A_0 - A_{-1} - t_1) + K_{30}A[2\delta_{10}(A_0 - t_1) + 2(t_{2,0} - t_{2,1})(A_0^* - t_1^*)] \\ &\quad - K_{30}A[-2\delta_{20}(A_0 - A_{-1}) + 2(t_{2,0} - r_{2,-1})(A_0^* - A_{-1}^*)] = 0, \end{aligned} \tag{B10}$$

$$m_0(-4\omega^2)t_{2,0} + k_0(2t_{2,0} - r_{2,-1} - t_{2,1}) + K_{30}A[(A_0 - t_1)^2 - (A_0 - A_{-1})^2] = 0, \tag{B11}$$

$$m_0(-9\omega^2)t_{3,0} + k_0(2t_{3,0} - t_{3,1} - r_{3,-1}) + K_{30}A[2(A_0 - t_1)(t_{2,0} - t_{2,1}) - 2(A_0 - A_{-1})(t_{2,0} - r_{2,-1})] = 0, \tag{B12}$$

$$m(-\omega^2)te^{2ika} + k_{\text{norm}}(2te^{2ika} - t_1 - te^{3ika}) = 0, \tag{B13}$$

$$m(-4\omega^2)t_2e^{2ik_2a} + k_{\text{norm}}(2t_2e^{2ik_2a} - t_{2,1} - t_2e^{3ik_2a}) = 0, \tag{B14}$$

$$m(-9\omega^2)t_3e^{2ik_3a} + k_{\text{norm}}(2t_3e^{2ik_3a} - t_{3,1} - t_3e^{3ik_3a}) = 0, \tag{B15}$$

$$m(-\omega^2)(e^{-2ika} + re^{2ika}) + k_{\text{norm}}(2e^{-2ika} + 2re^{2ika} - e^{-3ika} - re^{3ika} - A_{-1}) = 0, \tag{B16}$$

$$m(-4\omega^2)r_2e^{2ik_2a} + k(2r_2e^{2ik_2a} - r_{2,-1} - r_2e^{3ik_2a}) = 0, \tag{B17}$$

$$m(-9\omega^2)r_3e^{2ik_3a} + k(2r_3e^{2ik_3a} - r_{3,-1} - r_3e^{3ik_3a}) = 0, \tag{B18}$$

$$k_d(\delta_{1d} - \delta_{2d}) + K_{3d}A\left(\delta_{2d}^2 - \delta_{1d}^2 + 2|D_1 - t_1|^2 - 2|D_1 - A_{-1}|^2\right) = 0, \tag{B19}$$

$$-k_d\delta_{1d} - k_0\delta_{10} + K_{3d}A\left(\delta_{1d}^2 + 2|A_{-1} - D_1|^2\right) - K_{30}A\left(\delta_{10}^2 + 2|A_0 - A_{-1}|^2\right) = 0, \tag{B20}$$

$$k_d\delta_{2d} + k_0\delta_{20} - K_{3d}A\left(\delta_{2d}^2 + 2|t_1 - D_1|^2\right) + K_{30}A\left(\delta_{20}^2 + 2|A_0 - t_1|^2\right) = 0, \tag{B21}$$

$$k_0(\delta_{10} - \delta_{20}) + K_{30}A\left(\delta_{10}^2 - \delta_{20}^2 - 2|A_0 - t_1|^2 + 2|A_0 - A_{-1}|^2\right) = 0. \tag{B22}$$

We have 22 equations, Eqs. (B1)–(B22), on 22 variables. However, the last four equations yield zero in the l.h.s. in a sum, so we have effectively only 21 independent equations. But there is an additional condition on the equivalence of the total bond length change between the −1-st and +1-st atoms in the two wave paths in the atomic defect shown in Fig. 17:

$$\delta_{10} + \delta_{20} = \delta_{1d} + \delta_{2d}. \tag{B23}$$

Finally we have 22 independent equations on 22 variables.

APPENDIX C: DERIVATION OF LATTICE ENERGY TRANSMISSION AND REFLECTION COEFFICIENTS WITH AN ACCOUNT FOR HIGHER HARMONICS GENERATION AND PROPAGATION

The average in time flux of lattice wave energy in 1D discrete chain, which is given by the average scalar product of the force acting on and velocity of a particle, can be written as (see, e.g., [56])

$$J_E(\omega) = -\frac{1}{2}Re\left[\gamma(u_{n+1} - u_n)\frac{\dot{u}^*_{n+1} + \dot{u}^*_n}{2}\right], \tag{C1}$$

where u_n is a particle displacement from the equilibrium position in site n, and γ is a linear nearest-neighbor force constant. In the harmonic approximation, the displacements in the incident, i, and transmitted, t, plane waves are assumed to have the following form:

$$u_{n(i,t)} = (1, t)\exp(-i\omega t + ikan), \tag{C2}$$

where k is a wave number, a is a lattice period, and 1 and t are normalized amplitudes of the incident and transmitted waves. The flux of lattice energy, Eq. (C1), for the plane waves is reduced to

$$J_E(\omega) = -\tfrac{1}{4}\mathrm{Re}[\gamma(u_{n+1}\dot{u}^*_n - u_n\dot{u}^*_{n+1})], \tag{C3}$$

and we obtain the following expression for the energy flux in the incident and transmitted plane waves:

$$J_{E(i,t)}(\omega) = \tfrac{1}{4}(1, |t|^2)\omega^2\sqrt{m}\mathrm{Re}[\sqrt{4\gamma - m\omega^2}], \tag{C4}$$

where m is a particle mass in the monatomic chain, in which the phonon dispersion has the form $\omega = 2\sqrt{\gamma/m}\sin(ka/2)$.

Taking into account that the second and third harmonics of the incident wave have the frequencies 2ω and 3ω, the lattice energy transmission coefficient T_E, which is given by the ratio of the transmitted and incident lattice energies, has the following form that is used in Eq. (23a):

$$T = |t|^2 + 4|t_2|^2\mathrm{Re}\left(\sqrt{\frac{\omega^2_{\max} - 4\omega^2}{\omega^2_{\max} - \omega^2}}\right) + 9|t_3|^2\mathrm{Re}\left(\sqrt{\frac{\omega^2_{\max} - 9\omega^2}{\omega^2_{\max} - \omega^2}}\right), \tag{C5}$$

where t, t_2, and t_3 are the normalized transmission amplitudes of the main, second, and third phonon harmonics, respectively, in the frequency domain $0 \leqslant \omega \leqslant \omega_{\max}$, $\omega_{\max} = 2\sqrt{\gamma/m}$.

The lattice energy reflection coefficient R_E with an account for the propagation of higher harmonics can be derived in a similar way and has the following form that is used in Eq. (23b):

$$R = |r|^2 + 4|r_2|^2\mathrm{Re}\left(\sqrt{\frac{\omega^2_{\max} - 4\omega^2}{\omega^2_{\max} - \omega^2}}\right) + 9|r_3|^2\mathrm{Re}\left(\sqrt{\frac{\omega^2_{\max} - 9\omega^2}{\omega^2_{\max} - \omega^2}}\right), \tag{C6}$$

where r, r_2, and r_3 are the normalized reflections amplitudes of the main, second, and third phonon harmonics, respectively, in the frequency domain $0 \leqslant \omega \leqslant \omega_{\max}$, $\omega_{\max} = 2\sqrt{\gamma/m}$.

In a lossless system, the sum of the energy transmission and reflection coefficients should be equal to a unit, $T + R = 1$. Verification of the fulfillment of this condition is used in the main text for an accuracy check of the numerical simulations; see Fig. 4(b).

[1] Z. Wang, J. E. Alaniz, W. Jang, J. E. Garay, and C. Dames, Nano Lett. **11**, 2206 (2011).

[2] G. H. Zhu, H. Lee, Y. C. Lan, X. W. Wang, G. Joshi, D. Z. Wang, J. Yang, D. Vashaee, H. Guilbert, A. Pillitteri *et al.*, Phys. Rev. Lett. **102**, 196803 (2009).

[3] J. Maire, R. Anufriev, R. Yanagisawa, A. Ramiere, S. Volz, and M. Nomura, Sci. Adv. **3**, e1700027 (2017).

[4] C.-K. Hong, Z.-Y. Ou, and L. Mandel, Phys. Rev. Lett. **59**, 2044 (1987).

[5] C. Santori, D. Fattal, J. Vučković, G. S. Solomon, and Y. Yamamoto, Nature (London) **419**, 594 (2002).

[6] J. Beugnon, M. P. Jones, J. Dingjan, B. Darquié, G. Messin, A. Browaeys, and P. Grangier, Nature (London) **440**, 779 (2006).

[7] S. Wang, S. Mu, C. Zhu, Y. Gong, P. Xu, H. Liu, T. Li, S. Zhu, and X. Zhang, Opt. Express **20**, 5213 (2012).

[8] A. E. Miroshnichenko, S. F. Mingaleev, S. Flach, and Y. S. Kivshar, Phys. Rev. E **71**, 036626 (2005).

[9] Yu. A. Kosevich, Phys. Usp. **51**, 848 (2008).

[10] C. Lang, C. Eichler, L. Steffen, J. Fink, M. J. Woolley, A. Blais, and A. Wallraff, Nat. Phys. **9**, 345 (2013).

[11] Yu. A. Kosevich, Prog. Surf. Sci. **55**, 1 (1997).

[12] A. Fellay, F. Gagel, K. Maschke, A. Virlouvet, and A. Khater, Phys. Rev. B **55**, 1707 (1997).
[13] A. N. Darinskii and G. A. Maugin, Wave Motion **23**, 363 (1996).
[14] Yu. A. Kosevich and E. S. Syrkin, Phys. Lett. A **251**, 378 (1999).
[15] Yu. A. Kosevich, E. S. Syrkin, D. A. Semagin, and A. M. Kosevich, J. Exp. Theor. Phys. **90**, 974 (2000).
[16] Yu. A. Kosevich, L. G. Potyomina, A. N. Darinskii, and I. A. Strelnikov, Phys. Rev. B **97**, 094117 (2018).
[17] Yu. A. Kosevich, A. Feher, and E. Syrkin, Low Temp. Phys. **34**, 575 (2008).
[18] H. Han, L. G. Potyomina, A. A. Darinskii, S. Volz, and Yu. A. Kosevich, Phys. Rev. B **89**, 180301(R) (2014).
[19] Yu. A. Kosevich, H. Han, L. G. Potyomina, A. N. Darinskii, and S. Volz, in *Quodons in Mica*, edited by J. F. R. Archilla, N. Jiménez, V. J. Sánchez-Morcillo, L. M. García-Raffi (Springer, Cham, 2015), pp. 247–263.
[20] L. Feng, T. Shiga, H. Han, S. Ju, Yu. A. Kosevich, and J. Shiomi, Phys. Rev. B **96**, 220301(R) (2017).
[21] Yu. A. Kosevich and I. A. Strelnikov, in *Fourth International Conference on Quantum Technologies (ICQT-2017)*, AIP Conf. Proc. 1936 (AIP, Melville, NY, 2018), p. 020002, doi:10.1063/1.5025440.
[22] S. Hu, L. Feng, C. Shao, I. A. Strelnikov, Yu. A. Kosevich, and J. Shiomi, Phys. Rev. B **102**, 024301 (2020).
[23] Yu. A. Kosevich and I. A. Strelnikov, in *Fifth International Conference on Quantum Technologies (ICQT-2019)*, AIP Conf. Proc. 2241 (AIP, Melville, NY, 2020), p. 020023, doi:10.1063/5.0011386.
[24] Z. Liu, X. Zhang, Y. Mao, Y. Y. Zhu, Z. Yang, C. T. Chan, and P. Sheng, Science **289**, 1734 (2000).
[25] J. Li, X. Wen, and P. Sheng, J. Appl. Phys. **129**, 171103 (2021).
[26] S. Linden, C. Enkrich, M. Wegener, J. Zhou, T. Koschny, and C. M. Soukoulis, Science **306**, 1351 (2004).
[27] N. Liu, H. Liu, S. Zhu, and H. Giessen, Nat. Photonics **3**, 157 (2009).
[28] Yu. A. Kosevich, Phys. Rev. B **52**, 1017 (1995).
[29] N. Mingo, Phys. Rev. B **74**, 125402 (2006).
[30] J.-S. Wang, N. Zeng, J. Wang, and C. K. Gan, Phys. Rev. E **75**, 061128 (2007).
[31] K. Sääskilahti, J. Oksanen, J. Tulkki, and S. Volz, Phys. Rev. B **90**, 134312 (2014).
[32] J. Dai and Z. Tian, Phys. Rev. B **101**, 041301(R) (2020).
[33] Y. Guo, M. Bescond, Z. Zhang, M. Luisier, M. Nomura, and S. Volz, Phys. Rev. B **102**, 195412 (2020).
[34] L. Bonacina, P.-F. Brevet, M. Finazzi, and M. Celebrano, J. Appl. Phys. **127**, 230901 (2020).
[35] E. F. Page, M. J. Blake, G. A. Foley, and T. R. Calhoun, Chem. Phys. Rev. **3**, 041307 (2022).
[36] Yu. A. Kosevich, A. N. Darinskii, and I. A. Strelnikov, J. Sound Vib. **553**, 117663 (2023).
[37] A. Khelif, P. Deymier, B. Djafari-Rouhani, J. O. Vasseur, and L. Dobrzynski, J. Appl. Phys. **94**, 1308 (2003).
[38] Y. Pennec, B. Djafari-Rouhani, J. O. Vasseur, A. Khelif, and P. A. Deymier, Phys. Rev. E **69**, 046608 (2004).
[39] Yu. A. Kosevich, C. Goffaux, and J. Sánchez-Dehesa, Phys. Rev. B **74**, 012301 (2006).
[40] P. Schelling, S. Phillpot, and P. Keblinski, Appl. Phys. Lett. **80**, 2484 (2002).
[41] M. W. Klein, T. Tritschler, M. Wegener, and S. Linden, Phys. Rev. B **72**, 115113 (2005).
[42] Y. S. Joe, A. M. Satanin, and C. S. Kim, Phys. Scr. **74**, 259 (2006).
[43] A. E. Miroshnichenko, S. Flach, and Y. S. Kivshar, Rev. Mod. Phys. **82**, 2257 (2010).
[44] B. S. Luk'yanchuk, A. Z. B. Wang, B. A. E. Miroshnichenko, and C. W. Qiue, in *Singular and Chiral Nanoplasmonics*, edited by S. V. Boriskina and N. I. Zheludev (Pan Stanford Publishing, Singapore, 2015), pp. 285–309.
[45] M. F. Limonov, M. V. Rybin, A. N. Poddubny, and Y. S. Kivshar, Nat. Photonics **11**, 543 (2017).
[46] V. V. Smirnov, Int. J. Non Linear Mech. **142**, 104015 (2022).
[47] U. Fano, Phys. Rev. **124**, 1866 (1961).
[48] Q. Liu, Z. Yan, Y. Ao, and B. Wang, J. Appl. Phys. **132**, 060901 (2022).
[49] T. Markussen, J. Chem. Phys. **139**, 244101 (2013).
[50] C. L. Garrido Alzar, M. A. G. Martinez, and P. Nussenzveig, American J. Phys. **70**, 37 (2002).
[51] A. Barker Jr. and J. Hopfield, Phys. Rev. **135**, A1732 (1964).
[52] D. M. Riffe, Phys. Rev. B **84**, 064308 (2011).
[53] L. D. Landau and E. M. Lifshitz, *Mechanics* (Pergamon Press, Oxford, 1976).
[54] P. Jiang, Y. Ouyang, W. Ren, C. Yu, J. He, and J. Chen, APL Mater. **9**, 040703 (2021).
[55] S. Hu, Z. Zhang, P. Jiang, W. Ren, C. Yu, J. Shiomi, and J. Chen, Nanoscale **11**, 11839 (2019).
[56] L. D. Landau, E. M. Lifshitz, and L. P. Pitaevskii, *Electrodynamics of Continuous Media* (Butterworth-Heinemann, Oxford, 1984).